

THE STOICHIOMETRY AND KINETIC MODELING OF AN
ANAEROBIC BAFFLED REACTOR

by

Rebecca R. Erickson

A thesis submitted to the Faculty and Board of Trustees of the Colorado School of Mines in partial fulfillment of the requirements for the degree of Master of Science (Civil and Environmental Engineering).

Golden, Colorado

Date: _____

Signed: _____
Rebecca R. Erickson

Signed: _____
Dr. Linda A. Figueroa
Advisor

Golden, Colorado

Date: _____

Signed: _____
Dr. Terri S. Hogue
Professor and Head
Department of Civil and Environmental Engineering

ABSTRACT

The current domestic wastewater treatment paradigm is centered around aerobic biological treatment processes. The aerobic treatment of wastewater requires a substantial energy input, while effectively wasting a significant portion of the potential chemical energy found in the raw wastewater. This energy intensive process is perpetuated downstream of the aerobic treatment scheme due to its effectiveness in maximizing solids production- an added cost and energy component for digestion, dewatering, and exportation. Mainstream anaerobic treatment exhibits promising potential of becoming the sustainable wastewater treatment process of the future because of its energy generation potential from organics that are otherwise converted to solids under the current paradigm, lower input energy requirements, and reduced solids generation. A concern with mainstream anaerobic treatment of municipal wastewater is the potential impact of a lower water temperature on organic removal rates and lack of knowledge about the overall process stability in locations with temperate climates.

Anaerobic baffled reactors (ABRs) are essentially a series of compartments in which wastewater is directed through down-flow and up-flow conditions, passing through a solids layer that is retained in each compartment. This design allows for a decoupling of the solids and hydraulic residence time, meaning that solids are retained under varying hydraulic loading conditions. The ABR configuration fosters a naturally occurring spatial distribution of microorganisms that perform the sequential steps of hydrolysis, acidogenesis, acetogenesis, and methanogenesis, in the conversion of complex organic material to methane. An understanding of the stoichiometry and kinetics of an ABR receiving raw wastewater influent at ambient temperatures, is lacking. It is critical to develop this understanding in order to characterize the organic removal potential for further upscale and design of the ABR technology.

A unique data set was available from a four-compartment ABR located in the headworks building of Plum Creek Water Reclamation Authority in Castle Rock, CO, treated raw domestic wastewater for two years. The 1000-liter pilot reactor was operated at a 12-hour hydraulic residence time, treating the raw wastewater at ambient water and air temperatures as low as 12 °C. The data set was reduced to produce monthly averages of organics for particulate, dissolved and gas phase fractions. Four stoichiometric equations were developed based on model compounds. A simple reactor model with pseudo first order kinetics was fit to the monthly averages for measured and operationally defined organic fraction that were represented by model compounds. The model was used to relate the removal of different fractions of organic matter to process design and operation variables (e.g. volatile suspended solids, temperature).

In this study, eight parameters were used to describe the anaerobic degradation of soluble and particulate biodegradable substrate in the ABR, and three substrates were used to develop the stoichiometry. Modeling was used to evaluate how the processes of hydrolysis, fermentation, and methanogenesis are interrelated in each compartment based on the operationally defined organic fractions. Such analysis can provide a framework to better inform anaerobic reactor design and understanding.

TABLE OF CONTENTS

ABSTRACT.....	iii
LIST OF FIGURES.....	viii
LIST OF TABLES.....	xi
CHAPTER 1 INTRODUCTION AND LITERATURE REVIEW.....	1
1.1 Introductory Remarks.....	1
1.2 Background and Literature Review.....	5
1.2.1 Anaerobic Baffled Reactor Models.....	7
CHAPTER 2 MATERIALS AND METHODS.....	12
2.1 Materials and Methods.....	12
2.1.1 Anaerobic Baffled Reactor Description.....	12
2.1.2 Data Collection and Analysis.....	14
CHAPTER 3 MODELING OF THE STOICHIOMETRY AND KINETICS.....	15
3.1 Anaerobic Degradation Background.....	15
3.2 Simplifying the Anaerobic Degradation Pathway for the ABR.....	17
3.3 COD-Based Mass Balance.....	18
3.4 Stoichiometric Analysis.....	21
3.4.1 Hydrolysis: Cellulose the Model Polymer.....	22
3.4.2 Fermentation: Glucose the Model Monomer.....	23
3.4.2.1 Stoichiometry of Glucose Fermentation.....	24
3.4.3 Methanogenesis: The Selection of Acetate.....	26
3.4.3.1 Stoichiometry of Acetoclastic Methanogenesis.....	28
3.4.4 Stoichiometric Biomass Yield.....	29

3.5	Kinetic Analysis	30
3.5.1	Bulk Kinetic Parameters	31
3.6	Biosolids Movement within the ABR.....	33
CHAPTER 4 RESULTS AND DISCUSSION		36
4.1	Mass Balance Analysis	36
4.1.1	Error Analysis.....	37
4.2	Modeled Effluent pCOD versus Experimentally Determined Effluent pCOD.....	40
4.3	Modeled Effluent dCOD _{glucose} versus Experimentally Determined Effluent dCOD _{glucose}	43
4.4	Active Microbial Concentrations	46
CHAPTER 5 CONCLUDING REMARKS AND FUTURE RECOMMENDATIONS.....		53
5.1	Conclusion	53
5.2	Recommendations	54
REFERENCES CITED.....		55
APPENDIX A: METHANE CALCULATIONS		59
A.1)	Biogas Flowrate	59
A.2)	Measured Biogas Flowrate at Ambient Temperature to Biogas Flowrate at STP.....	61
A.3)	Percent Methane in the Biogas	63
A.4)	Dissolved Methane Concentration	65
A.4.1)	Oversaturation Calculation	65
A.4.2)	Henry's Constant Adjustment.....	67
A.4.3)	Total Dissolved Methane Concentration at Ambient and STP	67
A.5)	Percent Dissolved Methane	68
APPENDIX B: MODEL INPUTS AND FITTING PARAMETERS.....		70

B.1) Actual COD Concentrations and Cell 1 pCOD _{settled} Sink.....	70
B.1.1) Actual COD Concentrations.....	70
B.1.2) Cell 1 pCOD _{settled} Concentrations.....	74
B.2) K Values.....	75
B.3) Modeled pCOD _{cellulose} and dCOD _{glucose} Values.....	77

LIST OF FIGURES

Figure 2.1	Schematic of the anaerobic baffled reactor system at PCWRA.	13
Figure 3.1	The conversion of waste occurs in two stages. In the first stage, acid forming bacteria convert complex organics into organic acid. In the second stage, methane forming bacteria stabilize the organic acid by converting them into methane and carbon dioxide (Adapted from McCarty, 1964).....	15
Figure 3.2	The fate of biodegradable organics under anaerobic conditions (Adapted from Adekunle and Okolie, 2015).	16
Figure 3.3	The simplified anaerobic degradation pathway with three model substrates cellulose, glucose, and acetate representing complex organics, simple organics, and acids.	18
Figure 3.4	COD conversion pathways depicting the 3 major microbial functions: hydrolysis, acidification, and methanogenesis.	19
Figure 3.5	The mass balance approach used to analyze carbon flow through the system. Note: dCOD _{SRB, i+1} is a COD sink in Cell 1 alone, and dissolved CH ₄ only enters the system starting with Cell 1 effluent. The influent does not contain any dissolved methane.	20
Figure 3.6	The percentages of methanogens identified through DGGE and sequencing. Methanosaeta and Methanosarcina are indicators of an acetoclastic metabolism. Methanobacteriales and Methanomicrobiales are indicators of hydrogenotrophic metabolism (Hahn and Figueroa, 2016).	27
Figure 3.7	The sludge blanket volume shifts over time. Note, the December 2012 data represents the inoculum plus the growth of the solids layer from the time the ABR was inoculated in June 2012.	34
Figure 4.1	Cell 1 modeled effluent pCOD versus actual effluent pCOD concentrations. This Cell incorporates the pCOD _{settled} function found to exist from the mass balance.	41
Figure 4.2	Cell 4 modeled effluent pCOD versus actual effluent pCOD concentrations.....	42
Figure 4.3	Cell 1 modeled effluent dCOD _{glucose} versus experimentally determined effluent dCOD _{glucose} concentrations.	44
Figure 4.4	Cell 4 modeled effluent dCOD _{glucose} versus experimentally determined effluent dCOD _{glucose} concentrations.	45
Figure 4.5	MLVSS, in terms of g COD per L, of the core samples. As time progresses, the concentration of solids in the reactors shifts over time. Note, the	

September 2012 data is the inoculum plus the growth of the solids layer from the time the ABR was inoculated in June 2012.....47

Figure 4.6 (A) Year 1 and (B) Year 2 Kacetate versus MLVSS in which methane producing archaea concentrations are embedded in both the bulk kinetic parameter and MLVSS.....49

Figure 4.7 (A) Year 1 and (B) Year 2 Kglucose versus MLVSS in which fermenting bacteria concentrations are embedded in both the bulk kinetic parameter and MLVSS.....50

LIST OF TABLES

Table 1.1	Literature information of ABR operational parameters, model analysis parameters, and model equations.	6
Table 3.1	Yield and cell synthesis/electron coefficients for glucose and acetate substrates.	30
Table 3.2	VSS (g COD/day) entering and exiting the ABR pilot reactor P-Value found from monthly average VSS data for Year 1 and Year 2. The Year 1 and 2 average VSS concentration is shown for reference.	35
Table 4.1	Ratio of COD _{out} : COD _{in} based on monthly averages of COD entering and leaving the system. P values from the t-test indicate significant difference between the two years of study if P is less than 0.05.	36
Table 4.2	Average pCOD concentrations and average percent growth or removal of pCOD between Cells for influent through Cell 4.	38
Table 4.3	Net gain or net loss of MLVSS (g COD/day) from inoculation in Year 1 through Year 2 for Cells 1-4.	47
Table A.1	Biogas flowrate measurements over time.	59
Table A.2	Calculated biogas concentration based on temperature, over time. Percent difference is calculated for the measured total biogas flowrate versus the calculated biogas flowrate.	60
Table A.3	Total measured biogas flowrate at standard temperature and pressure over time.	61
Table A.4	Measured biogas flowrate at standard temperature and pressure for Cells 1-4 over time.	62
Table A.5	Percent methane in the biogas for Cells 1-4 over time.	63
Table A.6	Methane flowrate at standard temperature and pressure for Cells 1-4 over time.	64
Table A.7	Henry's constant (K_h) used to determine the dissolved methane concentration (DMC) at standard temperature and pressure from the ambient measurements, over time.	67
Table A.8	Percent dissolved methane concentration found from the DMC at standard temperature and pressure divided by the total methane flowrate at standard temperature and pressure, over time.	68

Table B.1	Influent concentrations of pCOD _{cellulose} , dCOD _{glucose} , and dCOD _{acetate} in units of mg COD/L. Note that the influent concentrations for methane and dissolved methane are zero.....	70
Table B.2	Average monthly experimentally determined data for Cell 1 in units of g COD/L. Note that pCOD consists of pCOD _{cellulose} and pCOD _{grease}	71
Table B.3	Average monthly experimentally determined data for Cell 2 in units of g COD/L.....	72
Table B.4	Average monthly experimentally determined data for Cell 3 in units of g COD/L.....	73
Table B.5	Average monthly experimentally determined data for Cell 4 in units of g COD/L.....	73
Table B.6	The Cell 1 monthly mass balance ratio and the monthly concentration of pCOD attributed to the gravitational settling function in units of g COD/L.....	74
Table B.7	Monthly K _{acetate} values determined for each Cell in units of 1/day.....	75
Table B.8	Monthly K _{glucose} values determined for each Cell in units of 1/day.....	76
Table B.9	Monthly K _{cellulose} values determined for each Cell in units of 1/day.....	76
Table B.10	Simulated pCOD _{cellulose} monthly concentrations in units of mg COD/L for Cells 1 through 4.....	78
Table B.11	Simulated dCOD _{glucose} monthly concentrations in units of mg COD/L for Cells 1 though 4.....	78

CHAPTER 1

INTRODUCTION AND LITERATURE REVIEW

1.1 Introductory Remarks

Wastewater has been recognized as a potential reservoir for recovering fertilizer, water, and energy; however, the processes used in conventional wastewater treatment are wasteful of both energy and recoverable resources (McCarty et al., 2011). Currently, the treatment of municipal wastewater focuses on what needs to be removed, as opposed to what can be recovered, while having an emphasis on energy intensive treatment processes (Guest et al., 2009). It is imperative for resource sustainability that conventional wastewater treatment move away from this wasteful paradigm to one that utilizes this renewable resource in a sustainable manner (Guest et al., 2009).

Conventional wastewater treatment revolves around an aerobic biological treatment process in which substantial energy input is required to provide oxygen for rapidly growing microbiota (Hahn and Figueroa, 2015; McCarty et al., 2011). Of the total energy utilized by a wastewater treatment plant (WWTP), approximately 50% of the energy is required for aeration (Mizuta and Shimada, 2010). This energy intensive aerobic process has an energy demand that is perpetuated downstream in solids treatment due to the large volume of biomass that is produced from aerobic treatment (Hahn and Figueroa, 2016). The biomass must be digested, dewatered, and exported, which result in large monetary and energy input requirements (Mizuta and Shimada, 2010).

In addition, aerobic treatment wastes much of the potential energy that can be produced from the carbon in the wastewater by converting about 50% to the large biomass volume, while the other 50% enters the atmosphere as CO₂ (Hahn and Figueroa, 2016). Replacing aeration with mainstream anaerobic treatment in a conventional WWTP exhibits promise of becoming the sustainable wastewater treatment process of the future. Mainstream anaerobic treatment has the potential to be an energy positive treatment process because of its ability to produce methane that can be used to generate energy from the carbon that is otherwise captured as solids or released as CO₂ under the current paradigm (Shoener et al., 2014). Mainstream anaerobic treatment has much lower energy input requirements and generates less solids than aerobic treatment (Barber and Stuckey, 1999; Shoener et al., 2014).

Mainstream anaerobic treatment of raw wastewater can be employed by a number of technologies; however, only three can be used for energy positive wastewater treatment. These technologies include an attached growth processes called the anaerobic fluidized bed (AFB), and two sludge blanket processes: the up-flow anaerobic sludge blanket (UASB) and the anaerobic baffled reactor (ABR) (Shoener et al., 2014). These three technologies are able to effectively treat raw wastewater and have the potential to be energy positive based on the required energy consumption and the theoretical energy yield (Shoener et al., 2014).

An AFB is a single tank reactor in which wastewater enters at high up-flow velocities in order to suspend a growth media located inside the reactor (Shoener et al., 2014). The treatment of wastewater is achieved through the degradation of substrate by the microorganisms that attach as a thin biofilm to the growth media (Shoener et al., 2014). Due to the AFB's inability to retain a large biomass volume, they are much more effective for treating low organic loading rates containing mostly soluble COD, where they are able to achieve a high percent COD removal

under these circumstances (Shoener et al., 2014). Though this technology has a promising high-percent energy recovery from degrading COD, called the energy yield (kJ/g COD) (Shoener et al., 2014), it has drawbacks. These drawbacks include the amount of energy required to fluidize the media, the long start up process for biofilm growth, the difficult reactor design and scalability, the lack of full-scale implementation in municipalities, and the expense of the media used (La Motta et al., 2008). Due to these shortcomings, the AFB was not investigated for the pilot study (Hahn and Figueroa, 2015).

A UASB is a single tank reactor in which wastewater is distributed across the base of the reactor where it must travel upward through the sludge blanket before it exits the reactor as effluent (Shoener et al., 2014). These reactors are advantageous due to their simple design and construction, small footprint, scalability, and proven application in full scale systems (Lettinga and Pol, 1991; Shoener et al., 2014). UASBs are also able to handle very high organic loading rates, especially when compared to the AFB (Lettinga et al., 1983); however, they are not able to achieve as high a percent COD removal as the ABR (Shoener et al., 2014). Also, the UASB's energy yield is much lower than that of the AFB or ABR (Shoener et al., 2014). Due to the lower percent COD removal and the much lower energy yield than the ABR, the UASB was not chosen for further investigation.

The ABR was developed by McCarty and colleagues in the early 1980's (Bachmann et al., 1982). The ABR is a series of sequential compartments in which wastewater is directed through a series of down-flow and up-flow conditions, passing upwards through each solids layer retained within each compartment (Bachmann et al., 1982). Like the UASB, ABRs have a simple design in which solids are retained in the reactor independent of the incoming wastewater, creating a decoupling of the solids and hydraulic residence time that allows for a retention of

solids under varying hydraulic loading conditions (Bachmann and Beard, 1985; Barber and Stuckey, 1999).

The ABR has been described as a series of UASBs, though it differs because the ABR configuration fosters a naturally occurring spatial distribution of microorganisms that perform the sequential steps of hydrolysis, acidogenesis, acetogenesis, and methanogenesis, in the conversion of complex organic material to methane (Hahn and Figueroa, 2015; Wang et al., 2004). ABRs can treat a large volume of solids without clogging, and the spatial dominance of microorganisms longitudinally through the reactor allows for the generation of biogas with higher methane concentrations in the downstream baffles (Bachmann et al., 1982; Wang et al., 2004).

Existing ABR models were developed using a bench-scale system receiving a completely soluble substrate feed at temperatures of 35°C. An understanding of the stoichiometry and kinetics of a pilot-scale ABR receiving raw wastewater influent at ambient temperatures, is lacking. This knowledge is critical for full-scale technology adoption by utilities receiving raw wastewater that contains both particulate and soluble substrate, in order to provide design guidance on organic substrate degradation through microbial consumption.

The goal of this study was to develop a model for an ABR using a minimum number of stoichiometric and kinetic parameters to describe organic degradation in each compartment. Understanding anaerobic systems like this on a fundamental level is imperative for their successful implementation and incorporation into conventional wastewater treatment.

1.2 Background and Literature Review

The ABR system has been modeled in a variety of ways, including Monod, first and second order models, the addition of biomass retention factors, sludge weights, inhibition, liquid mass transfer, and molecular diffusion, as seen in Table 1.1 (Bachmann et al., 1982; Bachmann and Beard, 1985; Li et al., 2016; Nachaiyasit and Stuckey, 1995; Skiadas et al., 2000; Stamatelatou et al., 2003; Xing et al., 1991). Though there are many models for the ABR system, none investigate the inter-compartment kinetics when a combined particulate and dissolved substrate, like wastewater, enters the system.

The inter-compartment kinetics of raw wastewater degradation are important for this system since each compartment contains mixed microbial populations of hydrolyzers, fermenters, and methanogens, with concentrations of those active microbial populations varying from compartment to compartment. The models to date are based on the use of readily biodegradable, soluble substrate; thus, they bypass the initial hydrolysis step of converting particulate COD into soluble COD during the anaerobic degradation process.

This control of completely soluble substrate allows for easier modeling; however, it does not provide a realistic investigation for implementation of the ABR in a wastewater treatment plant in which the raw wastewater consists of particulate and soluble organic and inorganic materials.

Table 1.1: Literature information of ABR operational parameters, model analysis parameters, and model equations.

Reactor Type	Substrate/ Feed	Process	Temp (°C)	Volume	Duration of Study (days)	Order	Model	Recycle Ratio	Substrate Model or Rate Equations	Reference
5 Compartment ABR	Nutrient broth and glucose	Continuous	35	Liquid: 6.3 L Total: 13 L	200	Variable Order	'Deep' Fixed-film reactor/ Monod	0-2.3	Non-Steady State: $\frac{dS}{dt} = -aCS^q + \frac{Q}{V}S^0 - \frac{Q}{V}S$ Steady State: $S = S^0 - \frac{a \cdot V}{Q} * CS^q$	Bachmann et al., 1982
5 Compartment ABR	Nutrient broth and glucose	Continuous	35	Liquid: 6.3 L Total: 13 L	223	Second Order	'Deep' Fixed-film reactor/ Monod	0-8	Non-Steady State: $\frac{dS}{dt} = -aCS^q + \frac{Q}{V}S^0 - \frac{Q}{V}S$ Steady State: $S = S^0 - \frac{a \cdot V}{Q} * CS^q$	Bachmann and Beard, 1985
3 Compartment Hybrid ABR (HABR)	Molasses Wastewater	Continuous	37	Total: 150 L	180	First Order	Series of CSTRs	0-10	$S = \frac{S^0}{(1 + \frac{k_1 W_1}{Q}) + (1 + \frac{k_2 W_2}{Q}) \dots (1 + \frac{k_n W_n}{Q})}$ $S = \frac{S^0 * (1+R)^{n-1}}{(1+R + \frac{k_1 W_1}{Q}) * (1+R + \frac{k_2 W_2}{Q}) \dots (1 + \frac{k_n W_n}{Q}) - (1+R)^{n-1} * R}$	Xing et al., 1991
4 Compartment Periodic ABR (PABR)	Glucose	Batch	35	Total: 15 L	100	First Order	CSTRs in series/ Monod plus Biomass Retention Factor	None	$r = \frac{\mu_{max} * S}{(K_s + S) * X}$	Skiadas et al., 2000
4 Compartment Periodic ABR (PABR)	Glucose	Batch	35	--	44	First Order	<METHANE>/ 2-part liquid and solid phase model/ inhibition factor	None	$r = \rho_{mj} * FT * FL * FI * X$	Stamatelatou et al., 2003
4 Compartment ABR	Brown Sugar Liquid	Continuous	35	Liquid: 28.4 L	110	First Order	IWA ADM1 plus Biomass Retention Factor/ inhibition factor	None	$\frac{dS}{dt} = \frac{Q * S^0}{V} - \frac{Q * S}{V} + \sum_{j=1-20} \rho_j \nu_{i,j}$	Li et al., 2016
4 Compartment ABR	Raw Wastewater	Continuous	12-23	Liquid: 870 L Total: 1000 L	730	Pseudo First Order	Monod Kinetics	None	$\frac{dS}{dt} = Q * S^0 - Q * S - k * S * V$	This Study

where S = bulk liquid substrate concentration (ML^{-3}), S^0 = influent concentration (ML^{-3}), C = variable-order reaction coefficient, a = specific surface area (L^{-1}), Q = flow rate (L^3T^{-1}), V = volume (L^3), q = variable-order reaction order, R = recycle ratio, W = mass of sludge (M), X = bacterial density (ML^{-3}), m_{max} = maximum specific consumption rate (MT^{-1}), K_s = saturation constant (ML^{-3}), k = bulk kinetic parameter (T^{-1}), X = total biomass concentration (ML^{-3}), r = consumption rate, ρ_{mj} = maximum specific rate of limiting substrate consumption, and FT , FL , FI = functions describing the dependence on temperature and the mechanisms of substrate limitation and inhibition.

1.2.1 Anaerobic Baffled Reactor Models

In 1982, a five-compartment ABR was modeled as a 'deep' fixed-film reactor in which an approximate, explicit solution for the flux of a limiting substrate into a deep fixed bacterial film could be provided. The organic loading rate (OLR) was increased from 2 to 20 kg COD/ m^3 *day, with COD removal ranging from 55-78% and higher removals seen at lower OLRs. The model incorporated liquid mass transfer, molecular diffusion, and Monod kinetics, using the steady-state equation found in Table 1.1 across the five-compartments. The model used an empirical approximation of Monod by incorporating four fitting parameters, including a variable order superscript (q) and a variable order constant that changed units based on the order (r). Overall, the model under predicted the amount of COD removal for all Compartments 1 through 5, which was attributed to the use of a recycle ratio. With an increase in loading and an increase in gas production in later cells, the diffusion depth layer would decrease as opposed to staying constant. A constant specific area (1/liters) was used for each of the five-compartments, which was not necessarily true, as an increase in mixing at higher loading rates would likely increase the area exposed to the substrate (Bachmann et al., 1982). The model was able to predict

effluent COD concentrations across the five-compartments when a recycle ratio was not incorporated.

Bachmann and Beard (1985) were able to support their initial hypothesis (Bachmann et al., 1982) that the ABR could be modeled as a 'deep' fixed-film reactor, using the same five-compartment ABR with added trace nutrients to the substrate feed as well as an additional eight fitting parameters. The OLR was increased from 11.4 to 36.2 kg COD/m³*day, with COD removal ranging from 55-91% and higher removals seen at lower OLRs. The increase in removal efficiency was attributed to the addition of trace nutrients. Unlike the model developed in 1982, the specific surface area was not kept constant in this adjusted model, and instead calculated as a fitting parameter for each of the five-compartments. The model was able to describe reactor performance between OLRs of 10.4 and 36 kg COD/m³*day (Bachmann and Beard, 1985). The model worked well to predict effluent COD concentrations with the eight additional fitting parameters.

Xing and colleagues (1991) developed a model for a three compartment hybrid ABR (HABR). In this HABR, the first two compartments were filled with 10 cm of plastic media at the liquid surface, and the last compartment had the upper half filled with a modular corrugated block (Xing and Tilche, 1992). The organic loading rate (OLR) was increased from 8 to 28 kg COD/m³*day, with COD removal ranging from 50 to ~90%, and higher removal rates seen at lower OLRs (Xing and Tilche, 1992). The HABR was assumed to be a series of completely mixed reactors, where all of the substrate utilization occurred in the granular sludge bed and the sludge bed was assumed to be completely mixed due to gas production (Xing and Tilche, 1992). ATP testing supported the assumption that substrate utilization occurred in the sludge bed of each compartment; thus, the mass of the granular sludge was used in place of the sludge

concentration (Xing et al., 1991). The model simulation showed consistent results with experimental data for the effluent COD predicted at OLRs between 2 and 25 kg COD/m³*day, though it did show stronger correlations at lower OLRs (Xing et al., 1991).

Skiadas and colleagues (2000) modeled a 15-L four-celled periodic ABR (PABR) fed in batches with glucose, under the assumption that the hydraulic behavior is equivalent to that of completely stirred tank reactors (CSTRs) in series, and that the biomass is retained through a constant retention factor. The role of the four cells of the PABR can be changed by switching the location of influent into the reactor, and in the extreme case of zero switching it acts as an ABR, while the other extreme of infinite switching would cause it to act like a UASB (Skiadas et al., 2000). The CSTR-based model combined the retention factor with Monod kinetics in order to predict the performance of a PABR that was developed earlier in 1998 (Skiadas and Lyberatos, 1998). When the PABR was operated without switching the influent location (operated as an ABR), the model was not able to accurately predict methane concentration when the HRT was changed from 10 to 2 days, attributed to methanogen washout occurring. The model predicted less methane production than what was observed in the experiment for all operational changes (zero switching through infinite switching), which was attributed to neglecting hydrogenotrophic methanogens (Skiadas et al., 2000). The usefulness of the model was not largely impacted by the lower methane concentration predictions, as the aim was to be able to predict the COD removal under different operational changes in order to optimize the PABR for the largest COD removal under varying OLRs. The model was able to accurately predict COD concentrations in each compartment, the effluent COD concentration, and the biomass concentration in the total PABR. Furthermore, the simulation predicts the PABR to perform better at high OLRs if it operated as a UASB and better at low OLRs if operated as a ABR (Skiadas et al., 2000)

Stamatelatou and Lyberatos (2002) investigated the performance of a 15-L four-celled PABR fed in batches with a protein substrate. The PABR was operated at OLRs between 3.125 and 6.25 kg COD/m³*day, at various HRTs. In this model, each compartment of the PABR was modeled as two separate variable-volume interacting sections of constant total volume, where one section is high in solids while the other is low in solids (Stamatelatou and Lyberatos, 2002). This allowed for the biomass retention to vary between the four-compartments, differing from the constant biomass retention factor seen in Skiadas et al., 2000. In 2003, Stamatelatou and colleagues adjusted the feed from protein to glucose; operating the PABR at OLRs between 3.125 and 18.75 kg COD/m³*day (Stamatelatou et al., 2003). The 2002 model was adapted to utilize the METHANE model that incorporates hydrogenotrophic and acetoclastic methane production (Vavilin et al., 1994). The METHANE model was adjusted to describe the kinetics of glucose degradation, and the oscillating effluent COD and VFA concentrations of the PABR performance under increasing OLRs was satisfactorily predicted (Stamatelatou et al., 2003). However, in order to work the model had to incorporate 35 model parameters under 40 varying biomass concentrations (Stamatelatou et al., 2003).

Li and colleagues (2016) set out to create a mathematical model of a 28.4 L four-compartment ABR fed a brown sugar liquid continuously over 110 days in which VFAs, COD, and biogas could be predicted under variable HRT conditions (Li et al., 2016). Percent COD removals averaged over 90% for all variations on HRT (1-2 days) at OLRs of 2 to 4 kg COD/m³*day, with the largest removals occurring in the first compartment (Li et al., 2016). A model was developed based on integrating liquid-gas mass transfer of biogas and a constant biomass retention factor (according to the methods of Skiadas et al., 2000) into the biochemical equations of the International Water Association (IWA) Anaerobic Digester Model No. 1

(ADM1) (Batstone et al., 2002; Li et al., 2016). Though Skiadas et al., (2000) and Stamatelatou et al., (2003) were able to simulate the PABR satisfactorily, the incorporation of hydrogenotrophic methanogenesis and liquid-gas mass transfer of biogas allowed this model to predict methane and biogas production more accurately (Li et al., 2016). The predicted VFAs, COD, and biogas values agreed well with the experimental data; however, a total of 26 kinetic/stoichiometric parameters, 27 dynamic state variables, and 24 equations for biochemical rates and physico-chemical processes were used to create the model (Li et al., 2016).

Though ABRs have been modeled in a number of ways, none are able to capture the inter-compartmental kinetics of an ABR in which non-soluble substrate, such as that present in raw wastewater, is fed into the reactor. All of the models presented contained readily biodegradable substrate, high influent COD concentrations, and were operated at 35 °C which does not provide an accurate representation of raw wastewater. Also, the ABRs investigated were all bench-scale as opposed to pilot-scale. As seen in Table 1.1, methanogenesis was assumed to be the rate limiting step in substrate degradation; however, if non-soluble substrate is present, hydrolysis is likely the rate limiting step due to the high solids and lipids concentration in the wastewater (Barber and Stuckey, 1999). Although the models presented in Stamatelatou et al., (2003) and Li et al., (2016) satisfactorily predicted reactor performance, they incorporated a large number of published and experimentally determined kinetic and stoichiometric parameters (Li et al., 2016; Stamatelatou et al., 2003). The purpose of this study was to minimize the number of stoichiometric and kinetic parameters used to describe the performance a pilot-scale four-compartment ABR receiving raw wastewater and operated at ambient water and air temperatures.

CHAPTER 2

MATERIALS AND METHODS

2.1 Materials and Methods

A four-compartment ABR was operated for two years (786 days) treating raw domestic wastewater from the Plum Creek Water Reclamation Authority (PCWRA) in Castle Rock, CO. The 1000-liter pilot reactor was operated continuously at a 12-hour hydraulic residence time, treating 1,728-liters/day of screened and de-gritted municipal wastewater. The ABR was located in the PCWRA Headworks building where it was exposed to ambient water and air temperatures (12- 23 °C, and -10-35 °C, respectively). The four compartments were spatially separated to provide room for sampling ports, instrumentation, and valves; a schematic is presented in Figure 2.1.

2.1.1 Anaerobic Baffled Reactor Description

The ABR was composed of four equally sized compartments (0.457 m width, 0.457 m length, 1.22 m height), from this point on, referred to as “Cells”. Each Cell had a nominal hydraulic volume of 220 L. Raw wastewater was introduced to the PCWRA headworks where it was first routed through a grinder sump pump and 8 mm screen. The screened and de-gritted wastewater was fed to a 910-liter continuously stirred reservoir tank, operated to maintain a maximum hydraulic residence time (HRT) of 15 minutes. Next, the wastewater was pumped from the reservoir tank into Cell 1 using a Watson Marlow peristaltic pump at a rate of 1.2 liters/minute. The HRT for each Cell was 3 hours, for a total system HRT of 12 hours.

The four Cells were equipped with a five-centimeter PVC downcomer pipe that directed influent wastewater from the reservoir tank or previous Cell, into the base of each Cell beneath the sludge blanket. The wastewater flowed upward through the sludge blanket then through a clarified zone at an upward velocity of 0.36 meters/hour, where it exited the Cell through an effluent pipe located just below the water surface. This hydraulic flow pattern was repeated for each Cell in the ABR. The Cells were constructed of PVC sheets that were reinforced with angle iron frames and each Cell was fitted with a gas flow meter, high-water-level alarm, temperature and pH probe. The pH over the course of the two-year study did not vary substantially, ranging between 6.5 and 7.2. The ABR was originally seeded in June 2012 with granular sludge from a mesophilic UASB that received brewing waste.

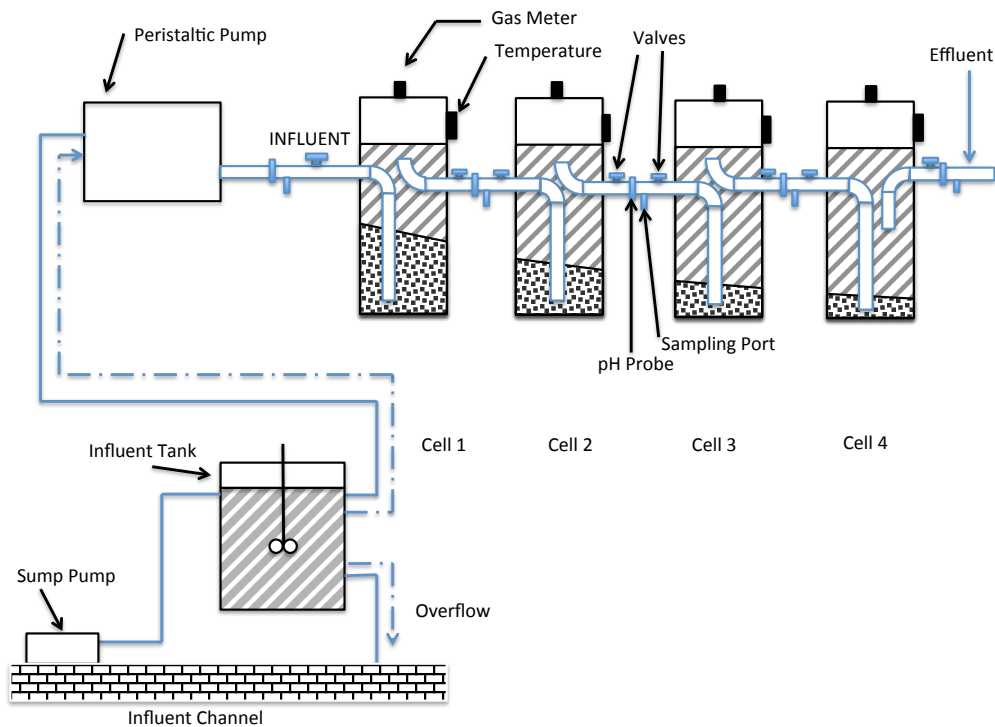


Figure 2.1: Schematic of the anaerobic baffled reactor system at PCWRA.

2.1.2 Data Collection and Analysis

Each Cell had grab samples analyzed according to the Standard Methods for total suspended solids (TSS), volatile suspended solids (VSS), total chemical oxygen demand (tCOD), dissolved COD (dCOD), particulate COD (pCOD), pH, alkalinity, volatile fatty acids (VFAs: acetate, propionate, oxalate, citrate, formate, and succinate), and biogas production and composition (CH_4 and CO_2) (APHA, 2005). Biogas flowrate, temperature, and pH were continuously monitored over the two-year study. Composite samples were collected periodically from the influent and Cell 4 to analyze TSS, VSS, tCOD, dCOD, pCOD, and alkalinity.

Quarterly, 3.8 cm core samples were taken from each Cell in order to determine solids and grease accumulation and composition. Temperature data was collected with a submersible HOBO Temp Pro V2. Broadly James pH ProcessProbes were used to collect pH data from influent through Cell 4. The biogas samples were collected with 2-liter Cali-Bond bags from the headspace of each Cell, and were analyzed for composition according to the methods described in Hahn and Figueroa (2015) using a Shimadzu GC-17A and Shimadzu GC-8A with TCD detectors and a HayeSep Q 80/100 column with UHP helium carrier gas at 30 mL/min. Biogas flowrate was measured using Cole Parmer 0 to 500 SSCM gas-flow meters on each of the four Cells. Dissolved methane was determined according to the methods described in Hahn and Figueroa (2015). The gaseous and dissolved methane calculations can be found in Appendix A.

CHAPTER 3

MODELING OF THE STOICHIOMETRY AND KINETICS

3.1 Anaerobic Degradation Background

Substrate undergoes anaerobic degradation in what was previously described by two separate stages (McCarty, 1964). In the first stage, anaerobic treatment of waste takes complex organics like carbohydrates, fats, and proteins and converts them into organic acids and hydrogen via acid forming bacteria. The organic acids and hydrogen are then transformed by methane forming bacteria to produce the stable end-products methane and carbon dioxide in the second stage (McCarty, 1964). In the first stage of this simplified process, hydrolysis and fermentation are the driving factors for the degradation of complex organics. In the second stage, methanogenesis is the driving factor behind the conversion of organic acids to methane and carbon dioxide, as seen in Figure 3.1 (Rittmann and McCarty, 2001).

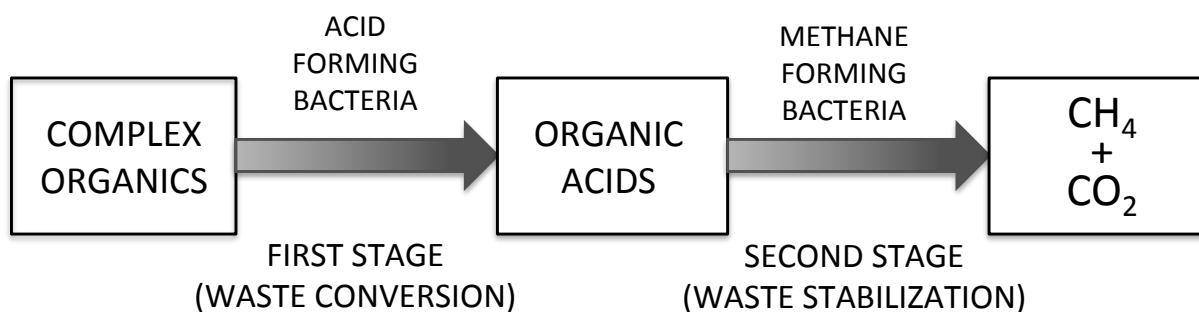


Figure 3.1: The conversion of waste occurs in two stages. In the first stage, acid forming bacteria convert complex organics into organic acid. In the second stage, methane forming bacteria stabilize the organic acid by converting them into methane and carbon dioxide (Adapted from McCarty, 1964).

As the understanding of the fundamentals of anaerobic processes increased, the degradation pathway was realized to be less of a two-stage system and more of a multi-step process of both parallel and series reactions (Bryant, 1979; Kaspar and Wuhmann, 1978). This new understanding explains the anaerobic degradation of waste in four steps: hydrolysis, acidogenesis, acetogenesis, and methanogenesis, as seen in Figure 3.2 below.

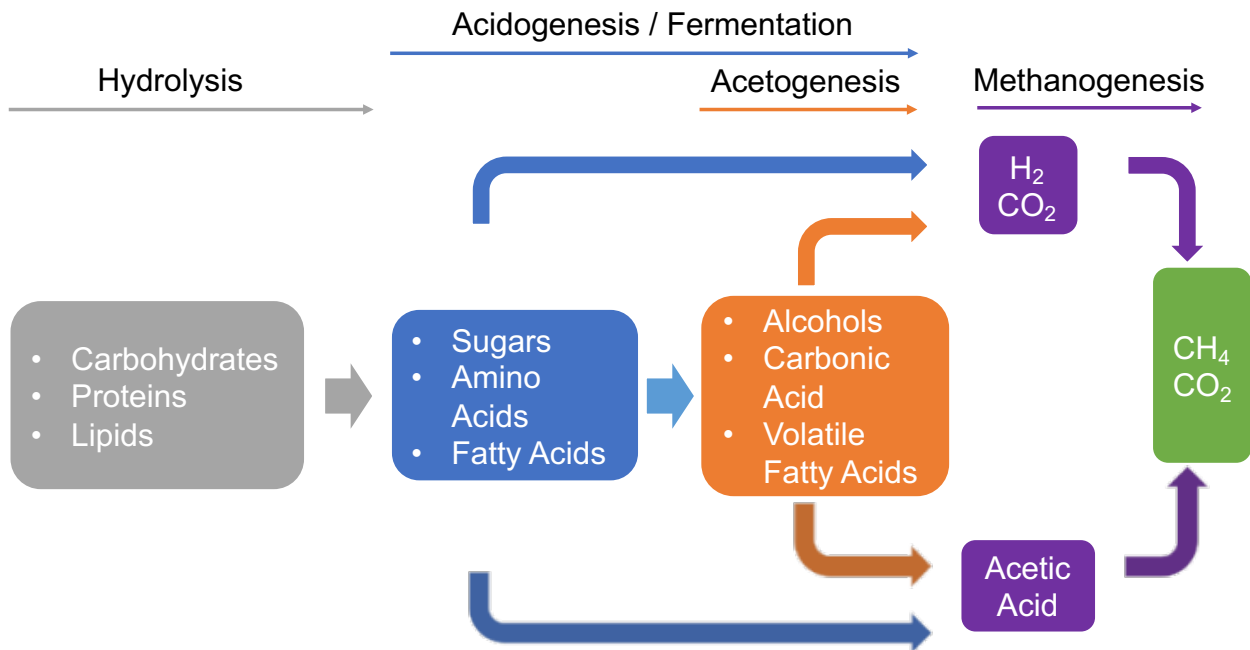


Figure 3.2: The fate of biodegradable organics under anaerobic conditions (Adapted from Adekunle and Okolie, 2015).

In the first step, complex particulate materials including carbohydrates, proteins, and lipids are hydrolyzed by extracellular enzymes, produced by multiple facultative and obligate anaerobes, creating soluble compounds that are small enough to transport across the cell membrane (Pavlostathis and Giraldo-Gomez, 1991; Tchobanoglous et al., 2014). These simpler,

soluble compounds are fermented by bacteria to produce volatile fatty acids (VFAs), carbon dioxide, and hydrogen in the second step of the process, acidogenesis. Within the acidogenesis process, substrates can be utilized as both electron acceptors and donors. Monosaccharides (sugars) and amino acids are predominately fermented into the VFAs: acetate, propionate, butyrate, as well as carbon dioxide and hydrogen. Low carbon fatty acids (LCFAs) fermentation produces acetate, carbon dioxide, and hydrogen. LCFA fermentation results in a larger fraction of COD conversion to hydrogen than that of sugars and amino acids (Tchobanoglous et al., 2014).

Within the fermentation process, acetogenesis is a subset of acidogenesis that specifically refers to the production of acetate from CO_2 and an electron source. Thus, the total fermentation process results in the production of acetate, carbon dioxide, and hydrogen, all of which are precursors for methanogenesis (Tchobanoglous et al., 2014). In the final step of the process, a community of Archaea organisms known as methanogens convert acetic acid and hydrogen into methane in a process called methanogenesis. Two groups of methanogenic organisms are responsible for methane production: acetoclastic methanogens and hydrogenotrophic methanogens. Acetoclastic methanogens are able to break acetate into carbon dioxide and methane, whereas the hydrogenotrophic methanogens utilize hydrogen as the electron donor and carbon dioxide as the electron acceptor to produce methane (Tchobanoglous et al., 2014).

3.2 Simplifying the Anaerobic Degradation Pathway for the ABR

In order to develop a minimum stoichiometry needed for kinetic analysis of the degradation of substrate within each Cell of the ABR, a systematic approach was utilized to

simplify the microbial degradation pathway shown in Figure 3.2. As stated, anaerobic microbial degradation follows the sequential steps of hydrolysis, acidogenesis, acetogenesis, and methanogenesis; however, this complicated degradation pathway was simplified approach as seen in Figure 3.3 below.

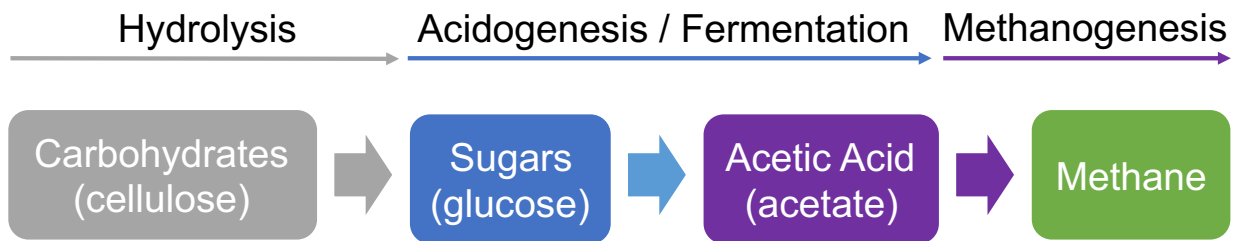


Figure 3.3: The simplified anaerobic degradation pathway with three model substrates cellulose, glucose, and acetate representing complex organics, simple organics, and acids.

Complex organics can be represented by carbohydrates, simple organics can be represented by sugars, sugars can be fermented into acetic acid, and acetic acid can undergo methanogenesis to methane alone. Carbohydrates, sugars, and acetic acid are represented by cellulose, glucose, and acetate. With this simplified pathway, a mass balance on the COD entering and exiting each Cell was investigated.

3.3 COD-Based Mass Balance

Raw wastewater contains both dissolved and particulate COD. In the simplified version of the anaerobic metabolism, COD degradation would follow that particulate COD hydrolyzes into dissolved COD, and some of the particulate COD goes unconverted and settles out. The

dissolved COD is transformed into volatile acids through acidifying, or fermenting, bacteria. The volatile acids undergo methanogenesis by acetoclastic methanogens, which release methane as a byproduct of degradation (Mosey, 1983). This COD conversion is shown in Figure 3.4.

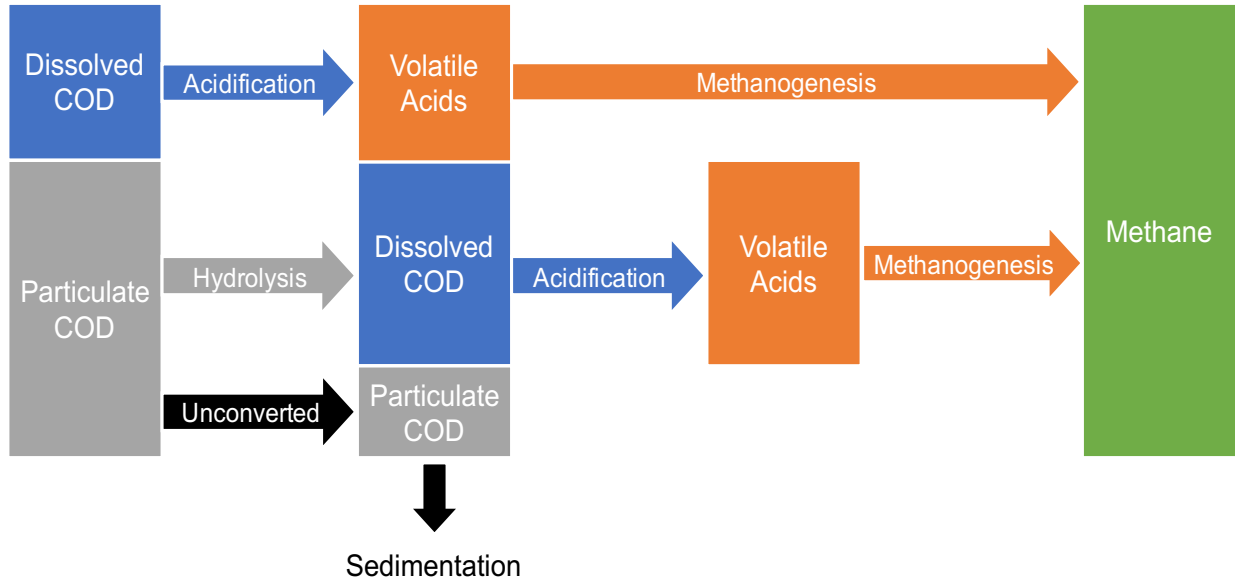


Figure 3.4: COD conversion pathways depicting the 3 major microbial functions: hydrolysis, acidification, and methanogenesis.

A COD-based mass balance, following the COD conversion pathway in Figure 3.4, was used to describe the intermediary substrate transformation within each of the four Cells. A monthly average was taken for each of the months August 2012 through July 2014 for the following parameters: pCOD, dCOD, acetate, propionate, dissolved methane, gaseous methane, grease, and for Cell 1 only, sulfate. All parameters were converted to units of g COD/day based on the convention used in other wastewater treatment biological models (Batstone et al., 2002;

Henze et al., 2015; Li et al., 2016; Vavilin et al., 1996). A visual representation of the mass balance model is shown in Figure 3.5 below.

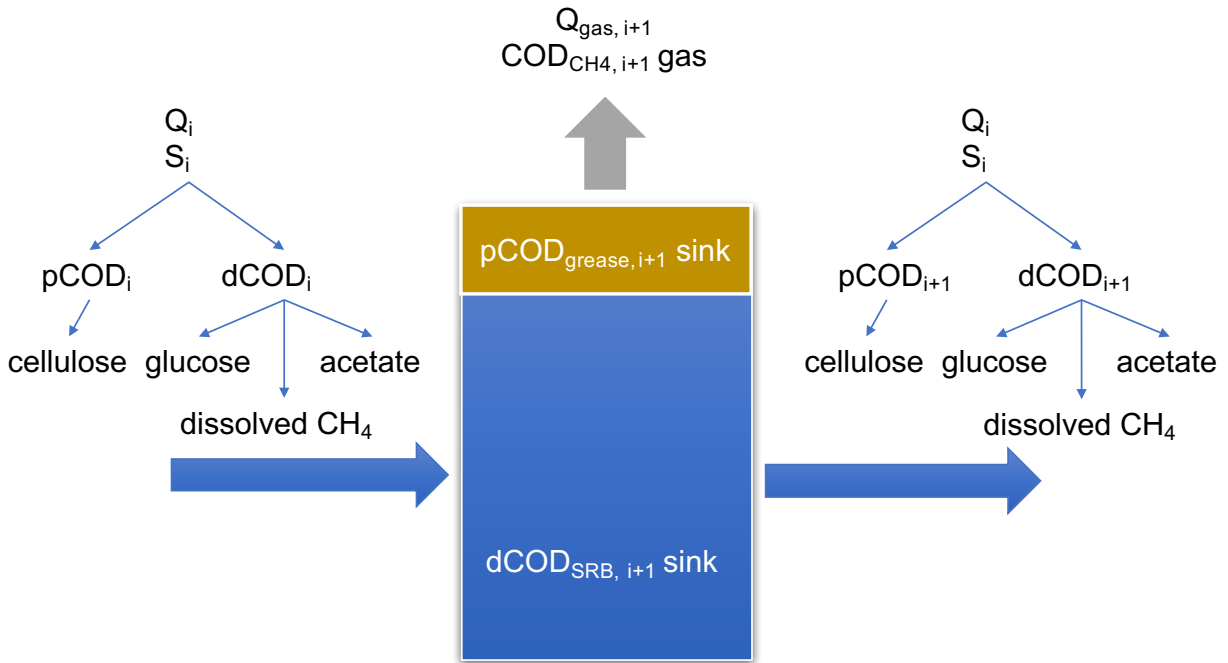


Figure 3.5: The mass balance approach used to analyze carbon flow through the system. Note: $dCOD_{SRB, i+1}$ is a COD sink in Cell 1 alone, and dissolved CH_4 only enters the system starting with Cell 1 effluent. The influent does not contain any dissolved methane.

In the mass balance, particulate COD was represented by the insoluble model compound, cellulose. Grease buildup in Cells 1-4 was represented as a particulate COD sink. Dissolved COD was assumed to be a combination of glucose and acetate equivalents, in which acetate equivalents were composed of measured acetate plus propionate concentrations. Glucose equivalents plus acetate equivalents was assumed to make up the total measured dissolved COD entering the system, thus the concentration of glucose equivalents was estimated from dissolved

COD minus acetate equivalents. Dissolved methane was assumed to be in addition to the measured the dissolved COD concentration; however, it only enters the ABR starting with Cell 2, as Cell 1 influent has not undergone methanogenesis. Due to the majority of sulfate reduction occurring in Cell 1 (data not shown), sulfate reduction was assumed to be associated with dissolved COD consumption in the first Cell alone. From Figure 3.5, Equation 3.1 was used to determine the ability of the mass balance to close.

$$\begin{aligned}
 & p\text{COD}_{\text{cellulose}, i} + d\text{COD}_{\text{glucose}, i} + d\text{COD}_{\text{acetate}, i} + (d\text{COD}_{\text{CH}_4, i}) = \\
 & p\text{COD}_{\text{cellulose}, i+1} + d\text{COD}_{\text{glucose}, i+1} + d\text{COD}_{\text{acetate}, i+1} + d\text{COD}_{\text{CH}_4, i+1} + g\text{COD}_{\text{CH}_4, i+1} \\
 & \quad + p\text{COD}_{\text{grease}, i+1} + (d\text{COD}_{\text{SRB}, i+1}) \tag{3.1}
 \end{aligned}$$

where $(d\text{COD}_{\text{CH}_4, i})$ only enters Cells 2 though 4, and $(d\text{COD}_{\text{SRB}, i+1})$ is a sink in Cell 1 alone.

The COD entering the system should equal the COD exiting the system. This should hold true between Cells, as well as for the overall system. From the simplified anaerobic degradation pathway, stoichiometries were developed for each of the assumed model substrates: cellulose, glucose, and acetate.

3.4 Stoichiometric Analysis

Three model substrates were selected to represent the particulate and dissolved COD entering and exiting each Cell within the ABR, gas phase and dissolved methane were combined for the stoichiometric analysis. As stated in the previous section, the model substrates were

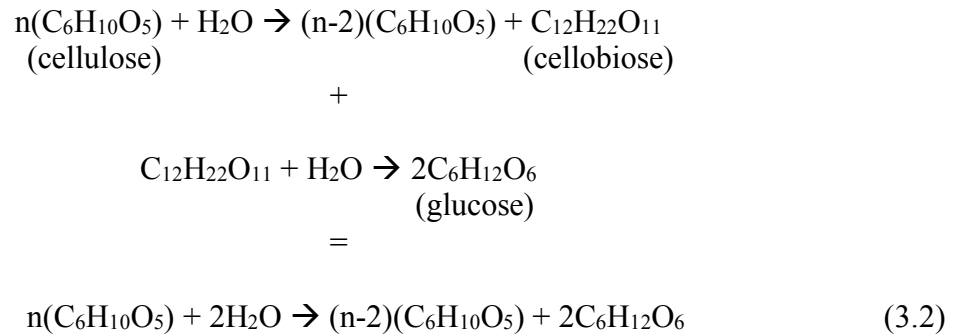
assumed to be cellulose, glucose, and acetate; where methane is the final product. The rationale for the selection of each substrate is described in the following sections.

3.4.1 Hydrolysis: Cellulose the Model Polymer

Hydrolysis is the first step in the depolymerization of organic matter (Christy et al., 2014). During this step the complex, insoluble organic substrate (carbohydrates, proteins, and lipids) undergo hydrolysis by facultative or obligate anaerobes that secrete a number of hydrolyzing enzymes that are then utilized by the anaerobes, degrading the substrate surface (Adekunle and Okolie, 2015; Christy et al., 2014). It has been reported by many researchers that hydrolysis is the rate limiting step due to the solid nature of the substrate (Adekunle and Okolie, 2015; Álvarez et al., 2008; Batstone et al., 2000; Vavilin, 1996). Polysaccharides like hemicellulose and cellulose occur in large amounts (60-70% dry weight) in many organic wastes (Hemsi et al., 2010), and cellulose has been used as the polymer describing the hydrolysis of complex carbohydrates (Batstone et al., 2000; Hemsi et al., 2010; Yu and Wensel, 2013). For the purpose of developing a stoichiometry-based kinetic model, cellulose was used as the simple polymer representing the entire hydrolysis step.

Cellulose is a simple polymer made of long chains of glucose molecules, covalently joined by beta bonds with neighboring chains typically linked together by hydrogen bonds in a crystalline structure (Wyman et al., 2004). Obligate anaerobes in the wastewater secrete different hydrolyzing enzymes (Christy et al., 2014). A number of enzymes can catalyze the reaction of water with the cellulose molecules to produce the disaccharide cellobiose (Christy et al., 2014; Wyman et al., 2004). The enzymes, called cellulases, can further catalyze the reaction of water

with the cellobiose molecules to produce the monosaccharide, glucose (Beguin and Aubert, 1994; Wyman et al., 2004), as shown in the following reaction:

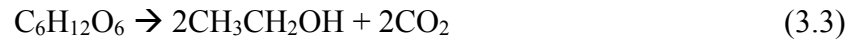


Many enzymes and microorganisms complicate the hydrolysis of cellulose to glucose, but for the purpose of this study, the simple conversion in the overall reaction was chosen (Beguin and Aubert, 1994).

3.4.2 Fermentation: Glucose the Model Monomer

Since the polysaccharide cellulose was chosen to represent the hydrolyzed complex organic substrate, for the purpose of developing a stoichiometric based kinetic model, it follows that glucose is the monosaccharide that undergoes acidogenesis, also called fermentation. Once the insoluble cellulose is hydrolyzed to glucose, it can be rapidly metabolized by a wide variety of fermenting bacteria, creating alcohols and organic acids, or bypass the acetogenesis step producing gases and acetic acid as seen in Figure 3.2 (Christy et al., 2014). Though the fermentation of glucose can produce organic acids, gases, and alcohols, models describing glucose fermentation in anaerobic wastewater treatment do not include intermediary ethanol production in acidogenesis, which will be explained later in this section (Batstone et al., 2002; Li

et al., 2016; Mosey, 1983). Three typical acidogenic reactions with glucose are as follows (Christy et al., 2014):

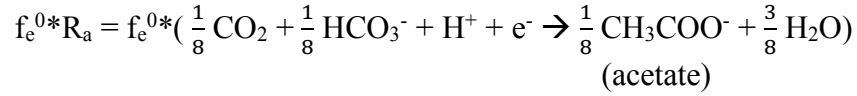


Equation 3.1 shows the conversion of glucose to ethanol. Equation 3.4 shows the conversion of glucose to propionic acid. Equation 3.5 shows the conversion of glucose to acetic acid. Though glucose can produce ethanol, propionic acid, and acetic acid, acetate was the chosen model compound to which glucose is fermented. Acetate is the conjugate base of acetic acid ($\text{pK}_a = 4.76$), and at the pH values in the ABR, acetate would be present. The selection of acetate was based on a few defining parameters that will be addressed in Section 4.2.3.

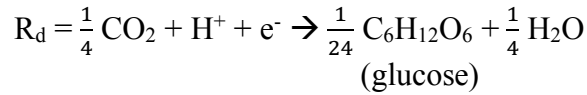
3.4.2.1 Stoichiometry of Glucose Fermentation

Once cellulose has been broken down into glucose, it is a readily accessible electron donor for fermenting bacteria. During cell synthesis, a portion of the electrons (f_e^0) from the electron donor is used to generate energy for the reduction of the electron acceptor, and the remaining portion (f_s^0) is used for cell synthesis. The sum of f_e^0 and f_s^0 is 1. In order to describe cell growth, three half reactions are required. One is needed to describe the oxidation of the electron donor (R_d), another for the reduction of the electron acceptor (R_a), and the last is needed to describe cell synthesis (R_c) (Rittmann and McCarty, 2001).

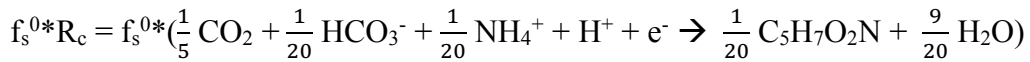
The half reaction for the electrons used for energy generation is $f_e^{0*}R_a$, where R_a is acetate.



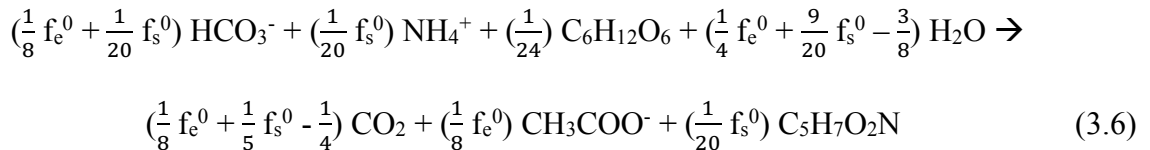
The electron donor half reaction is R_d , where R_d is glucose.



The cell synthesis half reaction (R_c) is dependent upon the nitrogen source. In this reaction, ammonium is the preferred nitrogen source due to its abundance in the influent wastewater. In order to produce biomass with the empirical formula used to characterize bacterial cells, $\text{C}_5\text{H}_7\text{O}_2\text{N}$ (Rittmann and McCarty, 2001), the synthesis half reaction is:

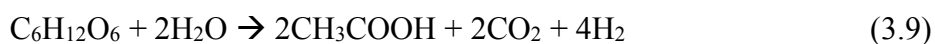
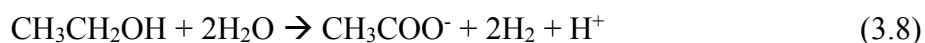


Thus, the total reaction (R) for fermentation is equal to: $f_e^{0*}R_a + f_s^{0*}R_c - R_d$



3.4.3 Methanogenesis: The Selection of Acetate

Bypassing acidogenesis and assuming that the fermenting bacteria reduced glucose to acetate alone was based on a few simplifying assumptions. The first is based on the fact that propionic acid, ethanol, and residual glucose left over from acidogenesis undergo a transformation in the presence of water to acetate, as seen in the equations below (Christy et al., 2014).



Equation 3.7 shows the conversion of propionate, the conjugate base of propionic acid (pKa = 4.88) to acetate, the conjugate base of acetic acid (pKa = 4.76). Equation 3.8 shows the transformation of ethanol to acetate. Equation 3.9 shows the conversion of glucose to acetic acid, which would become acetate under the pH conditions of the raw wastewater entering the ABR system. The reactions in Equations 3.7, 3.8, and 3.9 are imperative to the successful production of methane due to the fact that all volatile fatty acids and alcohols must be converted to acetic acid before they can be utilized by methane-producing archaea (McCarty and Mosey, 1991). Another reason for the selection of acetate was based on HPLC data showing that acetate and propionate were the dominant organic acid byproducts in all samples (Hahn and Figueroa, 2016). It should be noted that the sum of acetate and propionate concentrations were used, termed acetate equivalents.

Microbial analysis via qPCR and DGGE with sequencing by Hahn and Figueroa (2016) investigated the relative abundance of methanogens over the two-year pilot study. Figure 3.6 shows that acetoclastic methanogens were the most abundant in Cells 3 and 4 (69-74%) and were about half the methanogens in Cells 1 and 2 (48-59%). Due to the greater abundance of acetoclastic methanogens, the hydrogenotrophic metabolic pathway was not included in the model framework.

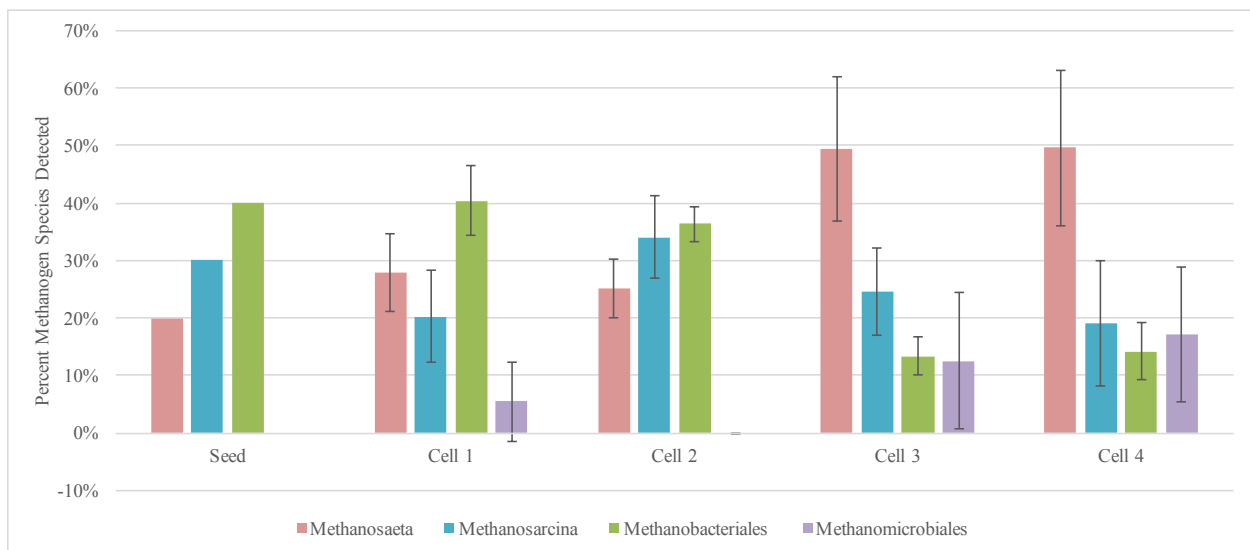


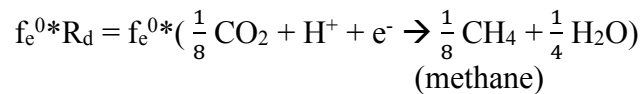
Figure 3.6: The percentages of methanogens identified through DGGE and sequencing. Methanosaeta and Methanosarcina are indicators of an acetoclastic metabolism. Methanobacteriales and Methanomicrobiales are indicators of hydrogenotrophic metabolism (Hahn and Figueroa, 2016).

Once glucose is broken down into alcohols and volatile fatty acids, under the given pH conditions, the acids produced were assumed to rapidly undergo acetogenesis to a final product of acetate. That acetate can then be used by the acetoclastic archaea to produce methane and carbon dioxide through methanogenesis (Mosey, 1983).

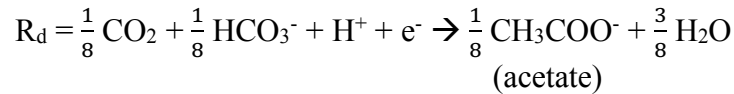
3.4.3.1 Stoichiometry of Acetoclastic Methanogenesis

Once glucose has undergone its transformation to acetate, that acetate can be reduced by methanogens, archaea microorganisms that live in close association with anaerobic bacteria, to produce methane and carbon dioxide in a process called methanogenesis. The three half reactions (R_d , R_a , and R_c) are required to describe cell growth.

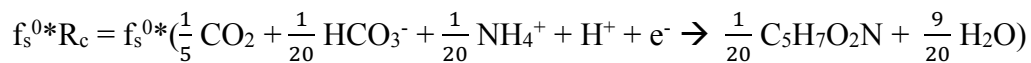
The half reaction for the electrons used for energy generation is $f_e^0 R_a$, where R_a is methane.



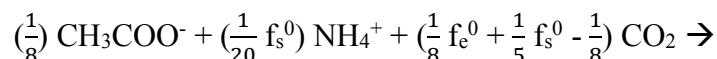
The electron donor half reaction is R_d , where R_d is acetate.

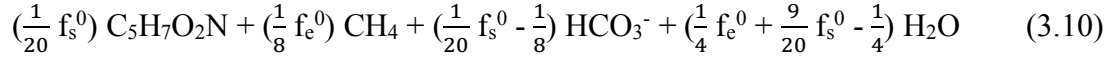


The cell synthesis half reaction can be described using the readily available ammonium as the nitrogen source.



Thus, the total reaction (R) for methanogenesis is equal to: $f_e^0 R_a + f_s^0 R_c - R_d$





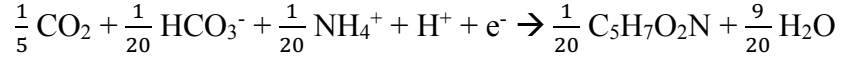
3.4.4 Stoichiometric Biomass Yield

The biomass yield in units of g biomass/g COD, can be estimated using the final stoichiometries developed for glucose and acetate found in Equations 3.6 and 3.10. The biomass synthesis yield is associated with the production of energy from the electron transfer from the donor to the acceptor (Rittmann and McCarty, 2001). The equation for determining the yield in mass units is as follows.

$$\text{Yield} = (f_s^0 * M_c) / (n_e * 8 \text{ g COD/e}^- \text{ eq donor}) \quad (3.11)$$

where M_c is the empirical formula weight of cells in g cells/mole cells, n_e is the number of electron equivalents in an empirical mole of cells in electron equivalents per mole of cell, and f_s^0 is the electron equivalents of cells per electron equivalents of the donor (Rittmann and McCarty, 2001).

In estimating the biomass yield, the nitrogen source is used to determine the electrons used in the synthesis half reaction of both fermentation and methanogenesis (Rittmann and McCarty, 2001). In anaerobic systems, the nitrogen will be in the form of ammonium (NH_4^+) since nitrate and nitrite are not present in raw wastewater. The biomass is represented by the empirical formula for bacterial microorganisms ($C_5H_7O_2N$) (Rittmann and McCarty, 2001). The cell synthesis half reaction (R_c) for ammonium and the creation of bacterial microorganisms can be seen below:



Based on the given information, $M_c = 113$ g cells/mole cells and $n_e = 20$ e⁻ equivalents/mole cells. Thus, the yield can be simplified to the following equation.

$$\text{Yield} = 0.706 * f_s^0 \quad (3.12)$$

Using thermodynamic estimation with an efficiency of 0.6, the following parameters were determined as shown in Table 3.1.

Table 3.1: Yield and cell synthesis/electron coefficients for glucose and acetate substrates.

Model Parameter	f_s^0	f_e^0	Yield (g Biomass/g COD)
Glucose	0.23	0.77	0.164
Acetate	0.06	0.94	0.043

Using the stoichiometry and yield calculations, quasi steady state pseudo-first order kinetics were derived for each of the three substrates, as well as the final product of methane.

3.5 Kinetic Analysis

A quasi steady-state pseudo-first order model was developed to describe the system using the simplified parameters from the stoichiometric analysis. Because the model inputs are monthly averages over the course of the two-years, the kinetics is referred to as “quasi steady-

state”. The purpose of the kinetic model is to use a minimum number of model parameters to describe the organic removal performance between Cells 1-4, as well as the overall system. The particulate and dissolved COD exiting Cells 1-4 was simulated.

3.5.1 Bulk Kinetic Parameters

Each of the three substrates described have a bulk kinetic parameter “K value” with units of 1/day used to describe the kinetics. These “K values” are labeled: $K_{\text{cellulose}}$, K_{glucose} , and K_{acetate} . $K_{\text{cellulose}}$ is a first order hydrolysis rate constant embedding active bacterial enzyme concentrations and temperature effects. Hydrolysis is typically modeled as a first order reaction (Ye and Berson, 2011). K_{glucose} and K_{acetate} are pseudo-first order approximations of Monod embedding active microbial concentrations. For K_{glucose} , those microbial concentrations are fermenting bacteria, and for K_{acetate} , the microbial concentration embeds the methane producing archaea.

To describe the kinetics of a dynamic system such as this, what the bulk kinetic parameters represent and what they are influenced by are imperative to understand. The following steady-state mass balance-based equations were developed to describe the apparent microbial substrate degradation pathways proposed using a pseudo-first order kinetic model. Note that the following equations use the notation that $i=0$ is the influent, $i=1$ is Cell 1, and so on.

1) Methane Production

$$0 = Q \cdot d\text{COD}_{\text{dissolved CH}_4, i} - Q \cdot d\text{COD}_{\text{dissolved CH}_4, i+1} - Q_{g, i+1} \cdot \text{COD}_{\text{gaseous CH}_4, i+1} + \gamma_{\text{CH}_4/\text{acetate}} \cdot K_{\text{acetate}, i+1} \cdot d\text{COD}_{\text{acetate}, i+1} \cdot V \quad (3.13)$$

2) Acetate Production

$$0 = Q \cdot d\text{COD}_{\text{acetate}, i} - Q \cdot d\text{COD}_{\text{acetate}, i+1} - K_{\text{acetate}, i+1} \cdot d\text{COD}_{\text{acetate}, i+1} \cdot V + \gamma_{\text{acetate}/\text{glucose}} \cdot K_{\text{glucose}, i+1} \cdot d\text{COD}_{\text{glucose}, i+1} \cdot V \quad (3.14)$$

3) Glucose Production

$$0 = Q \cdot d\text{COD}_{\text{glucose}, i} - Q \cdot d\text{COD}_{\text{glucose}, i+1} - K_{\text{glucose}, i+1} \cdot d\text{COD}_{\text{glucose}, i+1} \cdot V + \gamma_{\text{glucose}/\text{cellulose}} \cdot K_{\text{cellulose}, i+1} \cdot p\text{COD}_{\text{cellulose}, i+1} \cdot V \quad (3.15)$$

4) Cellulose Removal

$$0 = Q \cdot p\text{COD}_{\text{cellulose}, i} - Q \cdot p\text{COD}_{\text{cellulose}, i+1} - K_{\text{cellulose}, i+1} \cdot p\text{COD}_{\text{cellulose}, i+1} \cdot V - \zeta \cdot Q \cdot p\text{COD}_{\text{cellulose}, i} \quad (3.16)$$

where Q = liquid flowrate (L/day), Q_g = methane gas flowrate in Cell_{*i*+1} (L/day), V = Cell volume (L), $d\text{COD}_{\text{dissolved CH}_4, i}$ = dissolved CH₄ entering Cell_{*i*}, $d\text{COD}_{\text{dissolved CH}_4, i+1}$ = dissolved CH₄ exiting Cell_{*i*+1}, $\text{COD}_{\text{gaseous CH}_4, i+1}$ = gaseous CH₄ exiting Cell_{*i*+1}, $d\text{COD}_{\text{acetate}, i}$ = acetate entering Cell_{*i*}, $d\text{COD}_{\text{acetate}, i+1}$ = acetate exiting Cell_{*i*+1} (g acetate/L), $d\text{COD}_{\text{glucose}, i}$ = glucose entering Cell_{*i*}, $d\text{COD}_{\text{glucose}, i+1}$ = glucose exiting Cell_{*i*+1} (g glucose/L), $p\text{COD}_{\text{glucose}, i}$ = cellulose entering Cell_{*i*}, $p\text{COD}_{\text{cellulose}, i+1}$ = cellulose exiting Cell_{*i*+1} (g cellulose/L), $\gamma_{\text{CH}_4/\text{acetate}}$ = stoichiometric ratio of CH₄ production from acetate (g CH₄/g acetate), $\gamma_{\text{acetate}/\text{glucose}}$ = stoichiometric ratio of acetate production from glucose (g acetate/g glucose), $\gamma_{\text{glucose}/\text{cellulose}}$ = stoichiometric ratio of glucose production from cellulose (g glucose/g cellulose), ζ = monthly fraction of settled particulates in Cell 1 (unit less), $K_{\text{acetate}, i+1}$ = pseudo-first order rate constant of acetate conversion to methane in Cell_{*i*+1} (1/day), $K_{\text{glucose}, i+1}$ = pseudo-first order rate constant of glucose conversion to acetate in Cell_{*i*+1} (1/day), and $K_{\text{cellulose}, i+1}$ = first order rate constant of cellulose hydrolysis to glucose in Cell_{*i*+1} (1/day).

Equation 3.13 shows that dissolved methane enters a given Cell where it is lost through both the dissolved methane and gaseous methane exiting the Cell. Methane is produced through the consumption of acetate by methane producing archaea, noting the bulk kinetic parameter, K_{acetate} . The difference between the dissolved methane entering the system and the methane leaving as either dissolved or gas-phase is equivalent to the production of methane from acetate substrate consumption.

Acetate and glucose have similar equations, as seen in Equation 3.14 and 3.15. The dissolved substrate enters the Cell where it is lost through residual substrate exiting the Cell. Substrate is also lost through consumption, where it is consumed by either methane producing archaea (K_{acetate}) in Equation 3.14 or fermenting bacteria (K_{glucose}) in Equation 3.15. The substrate is produced by either the hydrolysis of cellulose ($K_{\text{cellulose}}$) in Equation 3.15, or the fermentation of glucose (K_{glucose}) in Equation 3.14. The difference between the substrate entering the Cell, leaving the Cell, and being consumed within the Cell, is equal to the amount of substrate being produced by either hydrolysis or fermentation.

In Equation 3.16, there is only degradation of cellulose substrate. It was assumed that all cellulose entering the system would either exit the cell, settle out, or degrade through hydrolysis. Note that for Cells 2-4, there is no fraction of the cellulose that was assumed to settle out; however, there was a transfer of pCOD that occurred across all Cells through solids migration.

3.6 Biosolids Movement within the ABR

It is well documented that ABRs retain solids largely independent of the incoming wastewater flow due to the nature of their design (Barber and Stuckey, 1999). This decoupling of SRT and HRT allows for a longer retention of biomass without a fixed-media or a separate solid

settling chamber, providing more time for the rate limiting hydrolysis step to take place (Barber and Stuckey, 1999). Though this configuration prevents a significant loss of solids, a discernable migration of solids was observed over the two-year pilot study as well as a periodic loss of solids as evidence by spikes in effluent values. There was no active solids-wasting over the two years. The migration of solids was incorporated indirectly in the mass balance through the monthly average pCOD concentrations, but its physical transfer was not included in the kinetic analysis.

The physical movement of solids was determined by measuring sludge volume once per quarter and documenting spikes in effluent COD concentrations. Figure 3.7 shows the accumulation and reduction of solids volume from Cell 1 through Cell 4.

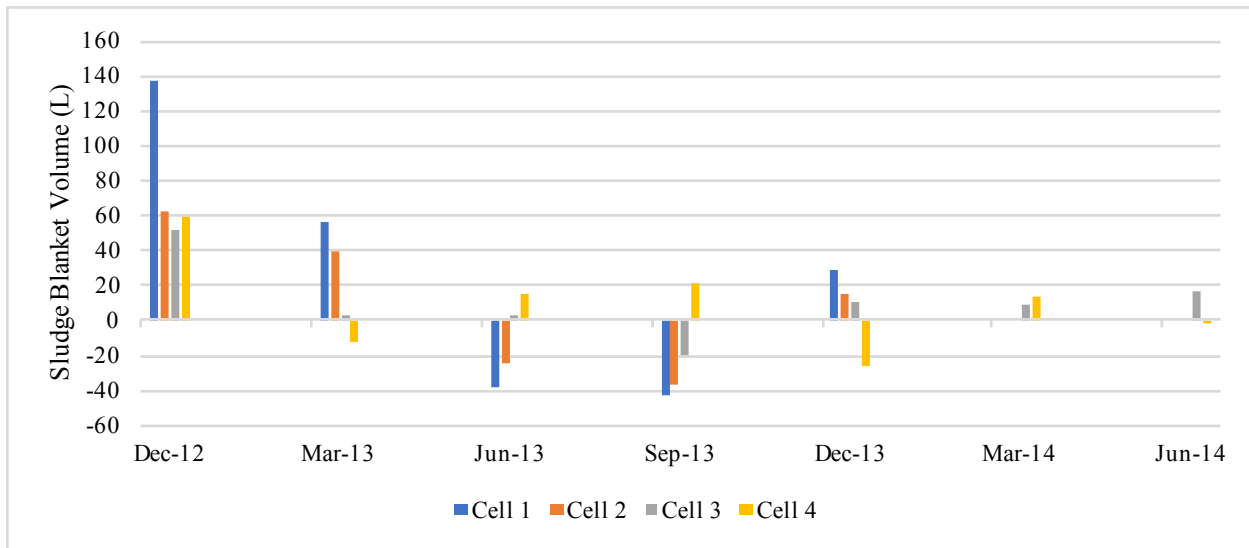


Figure 3.7: The change in sludge blanket volume over time. Note, the December 2012 data represents the inoculum plus the growth of the solids layer from the time the ABR was inoculated in June 2012.

Figure 3.7 shows a trend in solids migration of increasing and decreasing volume over time. This fluctuation in solids volume is not correlated to temperature or influent variations. The transfer of solids can increase or decrease the concentration of particulate COD that is retained in each Cell. A loss of solids as a result of effluent spikes, not migration, has been observed in pilot-scale UASB studies (G. Lettinga et al., 1983); and that trend is observed with the ABR as well, as seen in Table 3.2.

Table 3.2: VSS (g COD/day) entering and exiting the ABR pilot reactor P-Value found from monthly average VSS data for Year 1 and Year 2. The Year 1 and 2 average VSS concentration is shown for reference.

Location	Year 1 Average VSS	Year 2 Average VSS	Y1-Y2: P-Value from T-Test
Influent	845 ± 103	1006 ± 257	0.057
Cell 4 Effluent	125 ± 43	193 ± 44	0.001

Table 3.2 shows that the influent concentration of VSS (g COD/day) was not significantly different between the two years investigated. However, what left Cell 4 in Year 1 was statistically different than what left in Year 2. The Year 1 and Year 2 Average VSS columns show that the influent VSS concentration was more variable in the second year in terms of standard deviation, yet still was not significantly different from the first year. Cell 4, on the other hand, maintained a similar standard deviation in VSS concentration for the two years, but had a higher VSS concentration leaving the system. This loss of solids through effluent spikes is essentially unintentional particulate solids removal.

CHAPTER 4

RESULTS AND DISCUSSION

4.1 Mass Balance Analysis

Using Equation 3.1, monthly averages of COD concentrations in and out of each Cell were used in a quasi-steady state approach for the course of the two-year study. Because the model inputs are monthly averages over the course of the two-years, this approach is referred to as “quasi-steady state”. A t-test was performed, and a P value was calculated to determine the statistical difference in data from Year 1 to Year 2. As shown in Table 4.1, the Overall and Cell 2 COD mass balances indicated a lack of significant difference between Year 1 and Year 2 ($P > 0.05$); however, Cells 1, 3, and 4 suggested a significant difference between Year 1 and Year 2 ($P < 0.05$). Due to the statistically significant difference between the two years for the majority of the Cells, the two years were analyzed separately.

Table 4.1: Ratio of COD_{out} : COD_{in} based on monthly averages of COD entering and leaving the system. P values from the t-test indicate significant difference between the two years of study if P is less than 0.05.

Cell	Year 1 (Aug 2012-July 2013) Average COD _{out} /COD _{in} ± Standard Deviation	Year 2 (Aug 2013-July 2014) Average COD _{out} /COD _{in} ± Standard Deviation	P Value from T-Test for Two- Year Study
1	0.68 ± 0.06	0.59 ± 0.08	0.004
2	1.14 ± 0.14	1.07 ± 0.12	0.168
3	0.91 ± 0.08	1.03 ± 0.09	0.001
4	1.10 ± 0.07	1.21 ± 0.09	0.002
Overall	0.74 ± 0.05	0.74 ± 0.13	0.945

The COD-based mass balance in Table 4.1 shows that Cell 1 closed within ~32% in Year 1 and ~41% in Year 2, with a deficit in COD accounted for leaving the system. Cells 2, 3, and 4 closed within ~14% in Year 1 and ~21% in Year 2. Year 1 of Cell 2 maintained a deficit of COD accounted for entering the Cell; while Year 2 had months of both more and less COD accounted for in the effluent, as noted by the standard deviation. In the first year, Cell 3 had less COD observed in the effluent than influent, and in the second year, it had both more and less COD accounted for in the effluent, like Cell 2. The mass balance investigated reported more COD in the effluent than the influent in both years of Cell 4. The Overall mass balance closed within ~26% for both years, with a deficit in COD accounted for leaving the system.

The ABR is a biologically variable system with diurnally fluctuating influent that was assumed to have only seven parameters to account for all the COD entering and exiting each Cell. These parameters included: cellulose, glucose, acetate, dissolved methane, gaseous methane, grease, and sulfate reducing bacteria. This simple mass balance closed well for the Cells 2 through 4 (91 to 121% of the influent); however, the overall system and Cell 1 did not close as well as only 59 to 74% of the COD could be accounted for. Cell 1 was evaluated more carefully in order to determine reasons for the low COD in the effluent. An error analysis was conducted to help pinpoint this discrepancy in the mass balance.

4.1.1 Error Analysis

The inability to close the mass balance for the Overall system and Cells 1 through 4 completely can partly be attributed to measurement errors that propagate through the mass balance. Error associated with data collection and measuring devices is inherent to scientific analysis, and it is important to be considered.

The dissolved and particulate concentrations used in the COD mass balance were analyzed from grab samples that were collected at varying times each day. Grab samples can contain slugs of more or less COD based on the diurnal variations of the influent wastewater, and these difference, in tandem with inherent instrumentation errors, can be propagated throughout the mass balance. Gas chromatography analysis and HPLC analysis require an operator for both sample preparation and interpreting the results, introducing error associated with reported volatile fatty acid and gaseous methane concentrations. Grease samples and volume measurements were collected once per quarter; and that data had to be extrapolated to other months. The inherent error associated with sample collection, preparation, data interpretation, and measurement devices explain a portion of the inability to close the mass balance across the Overall system and Cells 1 through 4.

The results of the mass balance suggested that there was a pool of COD unaccounted for in the Cell 1. The deficit of COD in the Cell 1 effluent was attributed to a particulate COD sink occurring primarily in the first Cell. The average pCOD concentration and average percent pCOD removal for the two-year study is shown below in Table 4.2.

Table 4.2: Average pCOD concentrations and average percent growth or removal of pCOD between Cells for influent through Cell 4.

	Influent	Cell 1	Cell 2	Cell 3	Cell 4
pCOD (mg/L)	584 ± 108	212 ± 42	173 ± 38	166 ± 35	214 ± 70
% pCOD Removal	N/A	63 ± 8	16 ± 19	2 ± 20	-27 ± 22

Table 4.2 shows that Cell 1 had a particulate COD sink that was much greater than that of any other Cell. It should be noted that a negative percent removal of particulate COD represents a production of pCOD within the Cell. This large removal of pCOD, unique to Cell 1, was not completely accounted for in the mass balance. The $pCOD_{grease, i+1}$ sink did not account for a large enough loss in pCOD to close the balance, as shown in Equation 3.16.

The low ratio of COD_{out} to COD_{in} for Cell 1 shown in Table 4.1 was attributed to the pCOD sink that is occurring. In order to better model Cell 1, the missing portion of the COD ratio was attributed entirely to a $pCOD_{settled, i+1}$ function shown in the adjusted Cell 1 mass balance, 4.1.

$$\begin{aligned}
 & pCOD_{cellulose, i} + dCOD_{glucose, i} + dCOD_{acetate, i} = \\
 & pCOD_{cellulose, i+1} + dCOD_{glucose, i+1} + dCOD_{acetate, i+1} + dCOD_{CH_4, i+1} + gCOD_{CH_4, i+1} \\
 & + pCOD_{grease, i+1} + dCOD_{SRB, i+1} + pCOD_{settled, i+1}
 \end{aligned} \tag{4.1}$$

where $pCOD_{settled, i+1}$ is equal to $(1 - COD_{out}/COD_{in}) * pCOD_{cellulose, i}$ and the monthly varying $(1 - COD_{out}/COD_{in})$ term is equivalent to ζ presented in the pCOD removal, Equation 3.16.

This adjusted mass balance could not have been implemented without the investigation that provided the ratio of $COD_{out} : COD_{in}$; thus, the initial results were imperative to the success of the model. The adjusted mass balance allowed for Cell 1's $COD_{out} : COD_{in}$ to close at 0.92 ± 0.01 , and Cells 2 through 4 were not impacted. This $pCOD_{settled}$ mass occurring in Cell 1 was determined by the mass balance and was used to determine the settled pCOD removal efficiency coefficient for equation 3.16.

4.2 Model Inputs and Outputs

In the model analysis, actual influent pCOD concentrations were input into the Cellulose Removal equation to determine the Cell 1 effluent pCOD concentration. The Cell 1 simulated effluent was used as Cell 2 influent pCOD. This method was used for the remaining Cells. Influent experimentally determined $dCOD_{\text{glucose}}$ concentrations was used in the Glucose Production equation to simulate Cell 1 effluent $dCOD_{\text{glucose}}$ concentrations.

The actual COD concentrations used in this analysis, the derived K values, and the simulated monthly results are found in Appendix B. The actual COD concentrations were used in determining the mass balance, and the ratio of $COD_{\text{out}} : COD_{\text{in}}$ for Cell 1 found from the mass balance is shown to explain the $pCOD_{\text{settled}}$ gravitational settling function. The K value derivation is explained for each substrate as well as the values calculated for each bulk parameter. Finally, the results of the model are also shown for each month as well as the method used to determine them.

4.3 Modeled Effluent pCOD versus Experimentally Determined Effluent pCOD

Experimental data and model simulation results were compared for the particulate COD exiting each cell. This analysis was conducted in order to determine the effects of various influent particulate COD loadings ranging from 450 to 850 mg COD/L. The ABR effluent pCOD concentrations at different loadings was investigated. Results for simulated effluent pCOD concentrations versus experimentally determined pCOD concentrations for Cell 1 is shown in Figure 4.1 below.

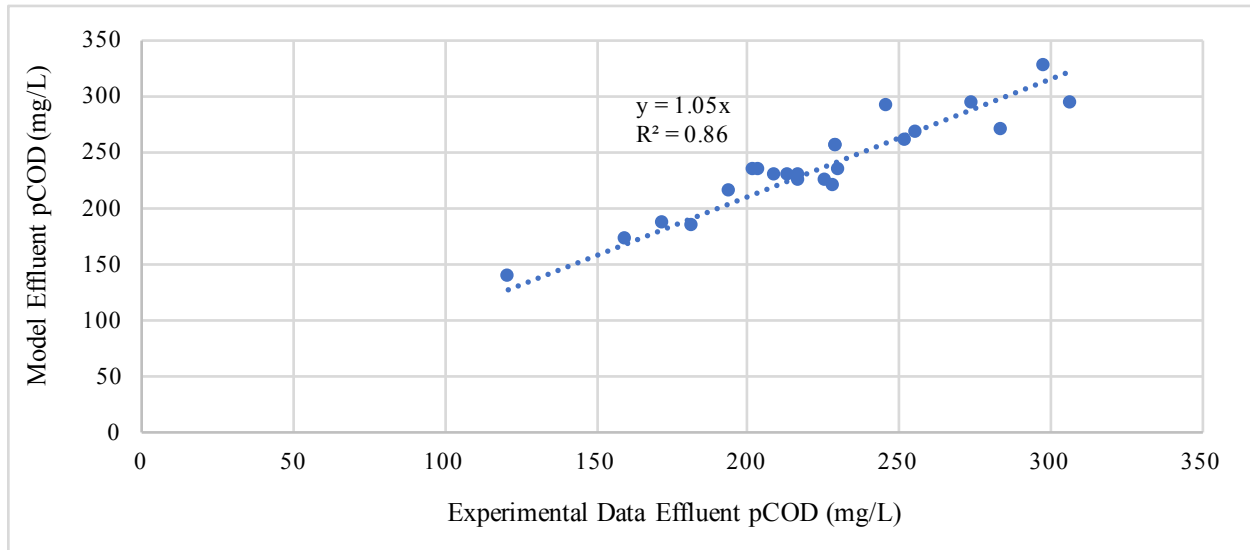


Figure 4.1: Cell 1 modeled effluent pCOD versus actual effluent pCOD concentrations. This Cell incorporates the $\text{pCOD}_{\text{settled}}$ function found to exist from the mass balance.

As shown in Figure 4.1, modeled pCOD exiting Cell 1 correlated well with experimentally determined pCOD effluent values. The origin was set through (0,0) and the equation on the graph shows that the modeled effluent pCOD was only 1.05 times greater than actual effluent pCOD. This minor over-prediction of effluent pCOD, or minor under-prediction of actual pCOD removal, is consistent with the mass balance closure that showed less measured COD accounted for in the effluent than influent (0.92 ± 0.01). The Cell 1 adjusted mass balance closed with more COD captured in the influent than the effluent, and those influent COD concentrations were used as inputs for the kinetic model.

The settled pCOD concentrations found from the mass balance were used in the hydrolysis kinetic analysis, shown previously in Equation 3.16. Overall, within the influent pCOD range of 450 to 850 mg/L, the model worked very well to predict the pCOD exiting Cell 1, especially when considering the inherent error in data collection and analysis, as well as the variability in this biological system.

The modeled effluent pCOD results in Cell 1 were used as the influent value of pCOD for Cell 2. The simulated effluent pCOD concentration in Cell 2 was used as the influent pCOD concentration for Cell 3, and so on through Cell 4. The modeled effluent pCOD versus the experimentally determined effluent pCOD concentrations were investigated for Cell 4, as shown in Figure 4.2 below.

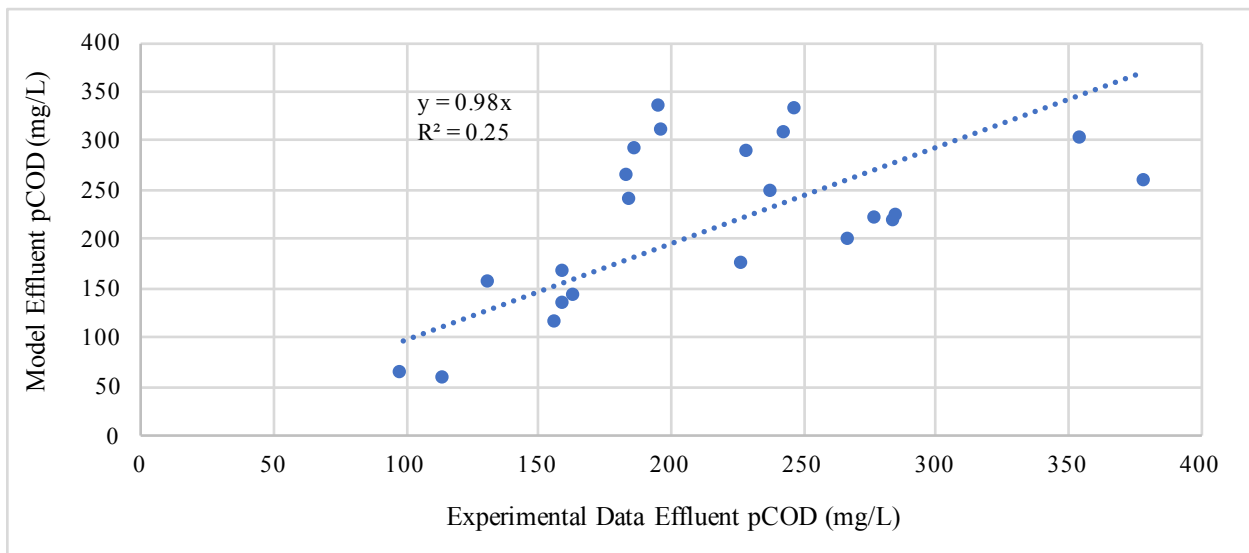


Figure 4.2: Cell 4 modeled effluent pCOD versus actual effluent pCOD concentrations.

As shown in Figure 4.2, the simulated pCOD concentration exiting Cell 4 did not have as strong a linear regression coefficient (R^2) as Cell 1. With that said, R^2 alone cannot explain a model's limitations or capabilities, though it can explain how well individual data points fit to a given equation (Fulton et al., 2008).

In this biological system, experimental data wavering from model predictions is expected due to factors unaccounted for, or yet to be discovered, that influence microbial performance. The origin was set to go through (0,0), and the model follows a similar upward trend shown in Figure 4.1. The modeled effluent pCOD is equal to 0.98 times the experimentally determined effluent pCOD concentrations.

As seen in Table 4.1, Cell 4 had a larger amount of COD accounted for in the effluent than in the influent, and the model predicted values that were slightly larger than the experimentally determined effluent pCOD concentrations. The slight under-prediction of pCOD removal in Cell 1 did not significantly impact downstream Cells, and Cell 4's actual effluent pCOD concentrations were closely predicted by the model, as seen in the equation on Figure 4.2. Under varying influent pCOD concentration, the model worked very well to predict the final effluent exiting the ABR.

4.4 Modeled Effluent $dCOD_{\text{glucose}}$ versus Experimentally Determined Effluent $dCOD_{\text{glucose}}$

Using the simulated effluent pCOD concentrations, the dissolved COD in the form of glucose was modeled for each Cell. The variables in this analysis were the influent $dCOD_{\text{glucose}}$ concentration which ranged from 100 to 175 mg COD/L, and the influent pCOD concentration that was used to determine effluent pCOD concentrations. The Cell 1 simulated effluent $dCOD_{\text{glucose}}$ concentration versus the experimentally determined $dCOD_{\text{glucose}}$ concentration is shown in Figure 4.3 below.

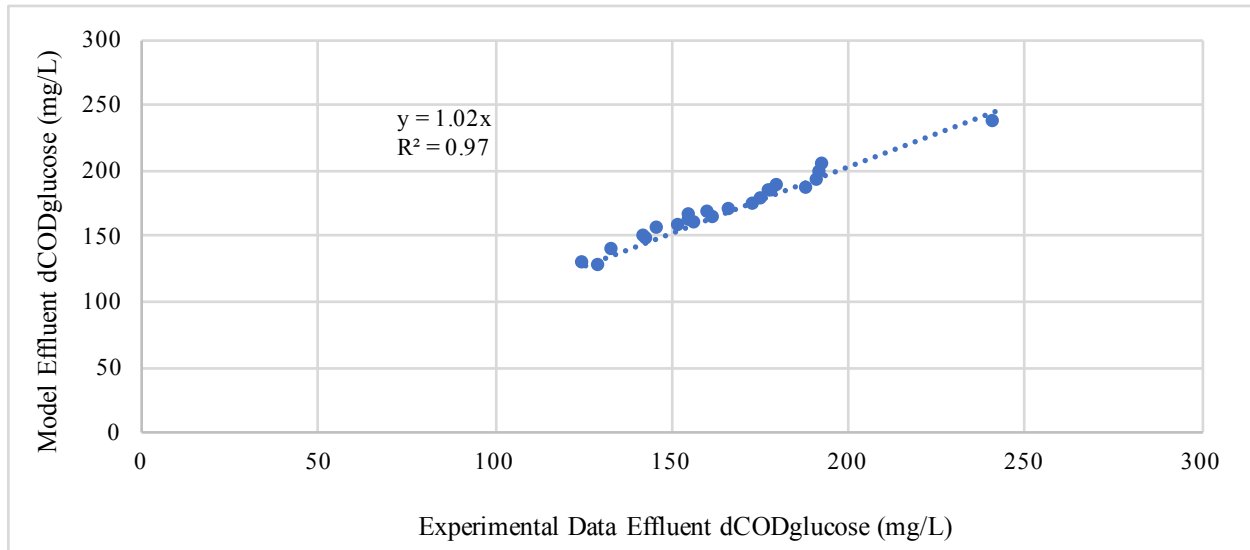


Figure 4.3: Cell 1 modeled effluent $dCOD_{glucose}$ versus experimentally determined effluent $dCOD_{glucose}$ concentrations.

The modeled effluent $dCOD_{glucose}$ concentrations was predicted using the bulk kinetic parameters, $K_{cellulose}$ and $K_{glucose}$, as well as the modeled effluent $pCOD$ concentrations from Section 4.2. As shown in Figure 4.3, the model was able to predict $dCOD_{glucose}$ concentrations that correlated well with experimentally determined values. With the origin set at (0,0), the modeled effluent $dCOD_{glucose}$ concentration was only slightly less than the experimentally determined values, noting the equation on the graph in which the model is equal to 1.02 times the experimental data.

As mentioned in Section 4.2, this slight over prediction of $dCOD_{glucose}$ removal results from the mass balance assumptions that resulted in more COD entering Cell 1 than exiting it. Overall, the model predicted effluent $dCOD_{glucose}$ consistent with experimentally determined values. The Cell 1 simulated effluent $dCOD_{glucose}$ concentration was used as influent for Cell 2, and so on through Cell 4.

The Cell 4 modeled effluent $dCOD_{\text{glucose}}$ versus the experimentally determined $dCOD_{\text{glucose}}$ concentrations can be seen in Figure 4.4 below.

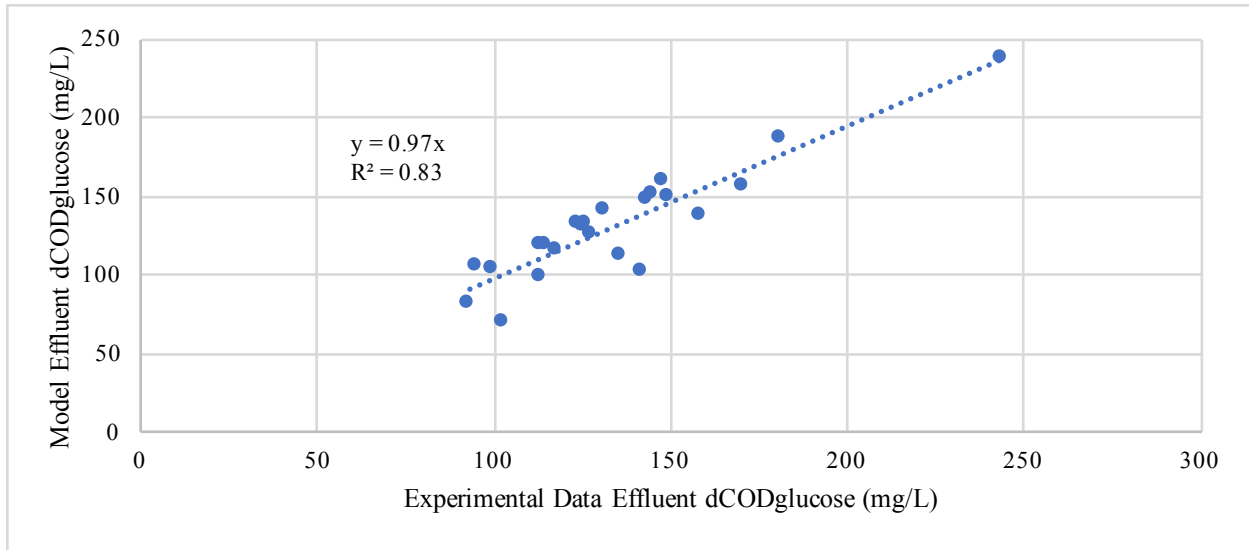


Figure 4.4: Cell 4 modeled effluent $dCOD_{\text{glucose}}$ versus experimentally determined effluent $dCOD_{\text{glucose}}$ concentrations.

As shown in Figure 4.4, the model slightly over predicted the actual effluent $dCOD_{\text{glucose}}$ concentration, based on the equation on the chart showing that the model equals 0.97 times the experimental data. The slight under prediction of actual $dCOD_{\text{glucose}}$ removal is consistent with the slight under prediction of actual pCOD removal. Since the modeled effluent pCOD concentrations were used to determine $dCOD_{\text{glucose}}$ concentrations, this slight inconsistency was propagated throughout the rest of the model.

As stated in **Section 4.2**, this is due to the initial assumptions in the mass balance resulting in less COD accounted for entering Cell 4 than exiting it. Considering that the $dCOD_{\text{glucose}}$ concentration was simulated using both simulated pCOD, K_{acetate} , and K_{glucose} data,

as shown in Appendix B, Cell 4 being predicted as close as it was shows that less variables added can work for a system such as the ABR. Overall, the model worked well to predict effluent $dCOD_{\text{glucose}}$ values for Cell 4, showing consistent results with experimentally determined values.

4.5 Active Microbial Concentrations

Section 4.2 and 4.3 proved that modeling the ABR with bulk kinetic parameters that encompass temperature and active microbial concentrations works well. In order for the kinetic model to accurately predict effluent pCOD and $dCOD_{\text{glucose}}$ concentrations, the mass balance of Cell 1 needed to incorporate a particulate COD settling function in which solids were retained at an inconsistent monthly ratio equivalent to ζ . The settling function allowed for pCOD to be accounted for that was not able to be traced in the mass balance, or through routine measurements that were taken. This alteration of the Cell 1 mass balance provided the understanding required to properly model the hydrolysis kinetics.

The movement of solids in Section 3.5 incorporates the movement of living and non-living organic biomass, and VSS can be used as a proxy for both the inert and active cell biomass existing in the sludge and migrating through the system (Rittmann and McCarty, 2001). Since the samples were collected in the form of a core sample, the VSS is referred to as mixed liquor VSS, or MLVSS. Figure 4.5 below shows the net gain and loss of MLVSS in grams of COD per liter.

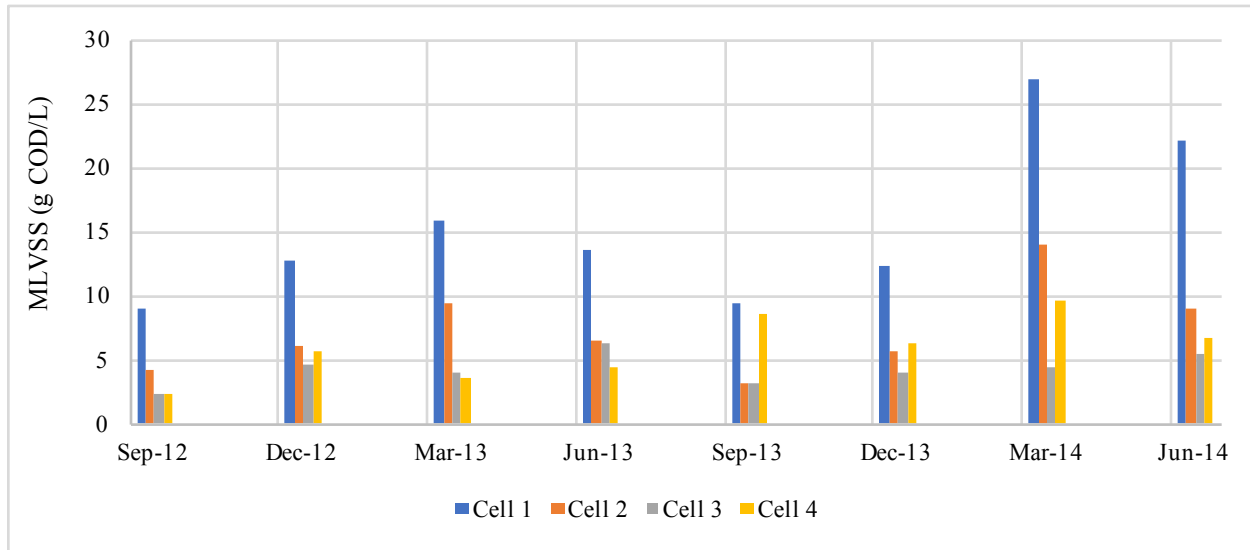


Figure 4.5: MLVSS, in terms of g COD per L, of the core samples. As time progresses, the concentration of solids in the reactors shifts over time. Note, the September 2012 data is the inoculum plus the growth of the solids layer from the time the ABR was inoculated in June 2012.

Figure 4.5 shows the MLVSS that can be gained or lost between the three months of each core sample measurement. The volatile portion of the solids represents the organic portion of the solids, and it can be used as a proxy for the active microbial populations (Ellis, 2004). The volatile solids concentration incorporates both inert and active organic biomass, so using it to determine active microbial populations is an approximation (Ellis, 2004; Rittmann and McCarty, 2001). A net gain of MLVSS was seen in Year 1 across all Cells, as shown in Table 4.3. In Year 2, there was a net gain of biomass for Cells 1, 2, and 4; and a slight decrease was seen for Cell 3.

Table 4.3: Net gain or net loss of MLVSS (g COD/L) from inoculation in Year 1 through Year 2 for Cells 1-4.

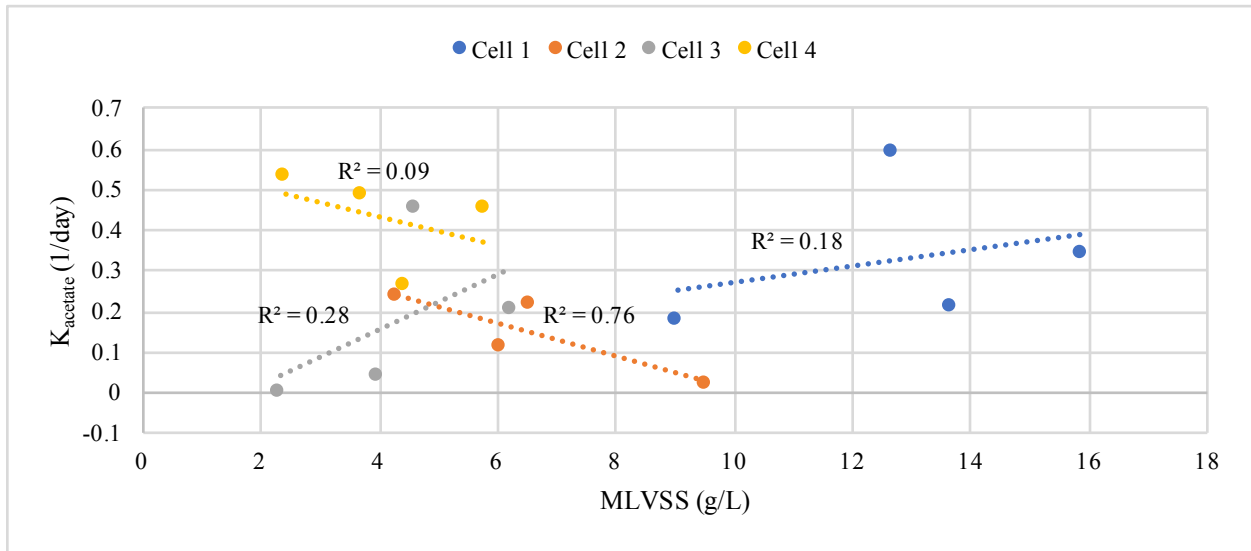
Timeframe	Cell 1	Cell 2	Cell 3	Cell 4	Overall
Year 1	13.7	6.6	6.2	4.4	30.9
Year 2	8.4	2.5	-0.7	2.3	12.5

In Year 1, the total net gain of solids was greater than that of Year 2. The percent reduction of solids gained between the first and second years are: Cell 1: 39%, Cell 2: 62%, Cell 3: 112%, and Cell 4: 48%. This indicates that in the first year, there was a greater buildup of active and inert biomass than in the second year, though there was still a net gain in MLVSS for Cells 1, 2, and 4 during Year 2.

The kinetic model was based on the assumption that the concentration of active microorganisms in a Cell would be related to the substrate consumption. Functions for solids migration and solids effluent spikes were not incorporated in the model. This transfer of solids from one cell to another should theoretically impact the bulk kinetic parameters, due to the transfer of biomass incorporating active biomass and substrate. This transferring of solids would not only transfer particulate COD, but it would also transfer active biomass from one Cell to the next.

In order to try to tease out the active microbial concentrations and find a relationship between “K values” and solids transfer, the bulk kinetic parameters were plotted against the MLVSS concentrations. Since MLVSS has been used as a proxy for active microorganisms in aerobic or activated sludge systems, the logic follows that active biomass concentrations should be able to be teased out. MLVSS was only analyzed for K_{acetate} and K_{glucose} , since they are the only bulk kinetic parameters that encompass active microorganisms: methane producing archaea and fermenting bacteria, respectively. Years 1 and 2 of K_{acetate} versus MLVSS are shown in Figure 4.6 below.

(A)



(B)

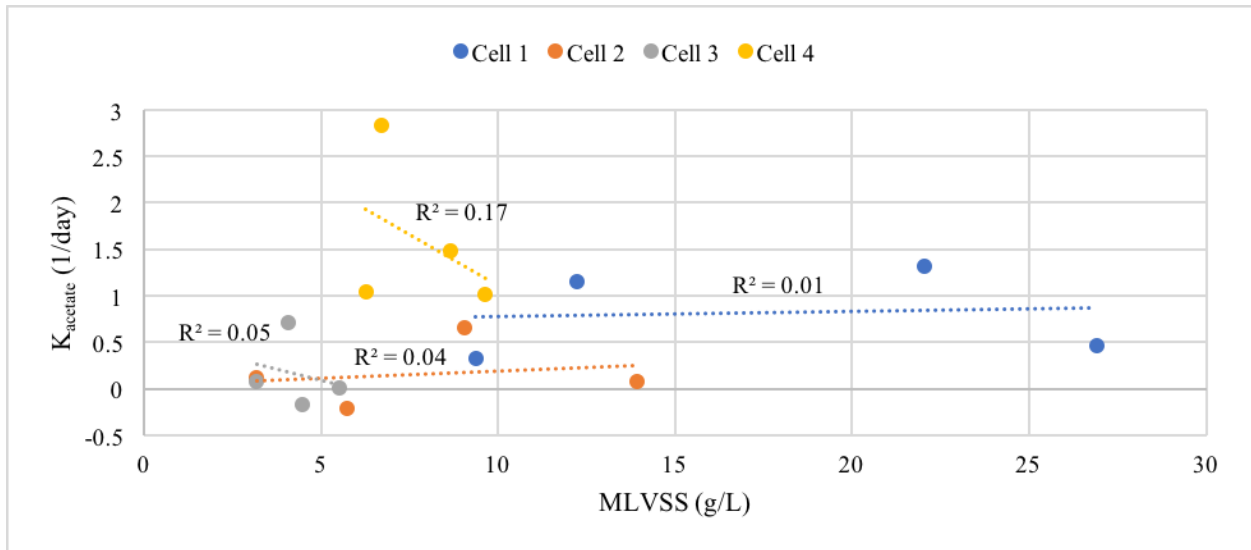


Figure 4.6: (A) Year 1 and (B) Year 2 K_{acetate} versus MLVSS in which methane producing archaea concentrations are embedded in both the bulk kinetic parameter and MLVSS.

As the MLVSS concentration increases, it would be expected that the bulk kinetic parameters would increase as well. Since K_{acetate} and MLVSS both contain active methane

producing archaea, teasing out that active microorganism concentration was thought to be possible through this analysis.

As shown in Figure 4.6 (A), Cells 1 and 3 had data that followed the assumed upward linear trend line; however, Cell 2 and 4 did not. In Figure 4.6 (B), Cells 1 and 2 showed a very slight upward trend, and Cells 3 and 4 were trending toward a decrease in K_{acetate} with an increase in MLVSS. A similar phenomenon is shown in Figure 4.7 below with K_{glucose} versus MLVSS.

(A)

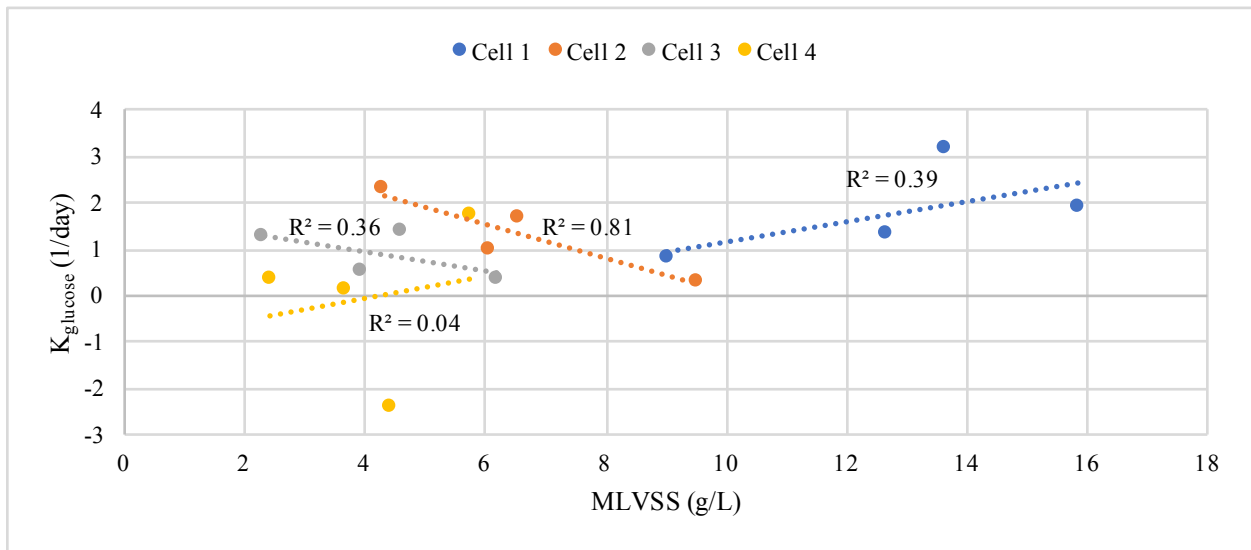


Figure 4.7a: Year 1 of K_{glucose} versus MLVSS in which fermenting bacteria concentrations are embedded in both the bulk kinetic parameter and MLVSS.

(B)

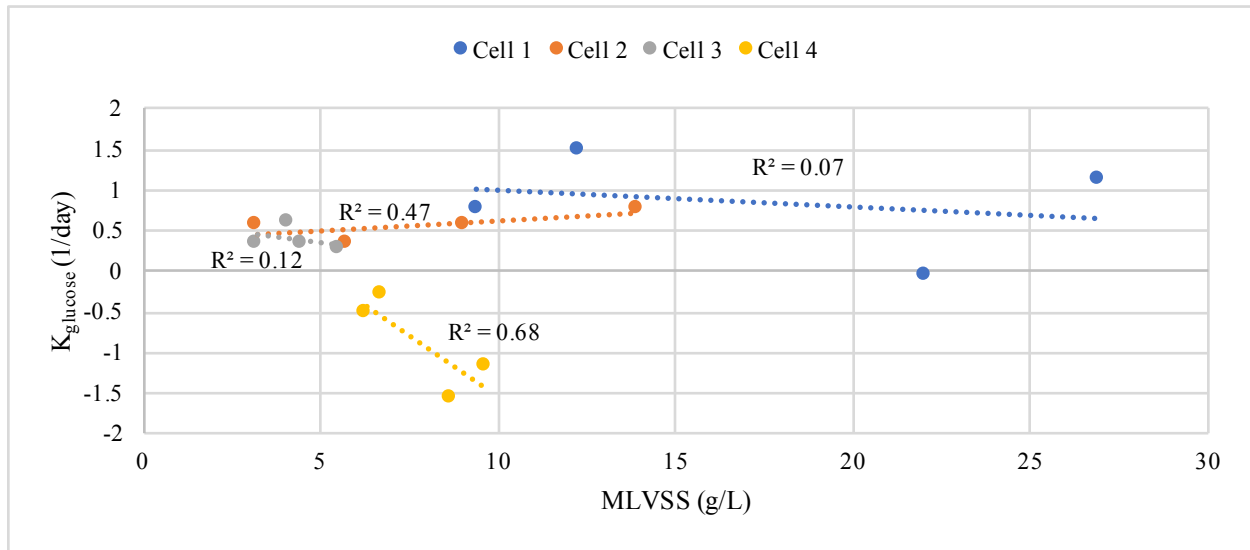


Figure 4.7b: Year 2 of $K_{g,glucose}$ versus MLVSS in which fermenting bacteria concentrations are embedded in both the bulk kinetic parameter and MLVSS.

If MLVSS was a reasonable proxy for active microorganisms the first order bulk kinetic parameters would have a positive linear correlation with MLVSS. In Figure 4.7 (A), Cells 1 and 4 have positive correlation with MLVSS, and Cells 2 and 3 have negative correlations. Figure 4.7 (B) shows a negative trend for Cells 1, 3, and 4 and a positive trend for Cell 2. Overall, MLVSS was a poor proxy for both fermenting bacteria and methane producing archaea across all Cells in the ABR. Using MLVSS as a proxy for active microorganisms works well in determining the Food to Mass Ratio in activated sludge processes that require aeration; however, in anaerobic systems, MLVSS does not appear to correlate to the active microorganisms.

Part of the reason MLVSS does not correlate to active microorganisms can be attributed to the lack of a constant or quantifiable Mean Cell Residence Time (MCRT). MCRT is used in activated sludge systems in order to determine the age of the sludge; however, in this ABR without solids wasting, MCRT cannot be quantified. MCRT is not equivalent to the solids

residence time (SRT) in a system receiving influent particulate matter that contains organic, inorganic, active, and inert biomass; though MCRT and SRT are equivalent in activated sludge processes. Unlike activated sludge, the SRT of the ABR system was not constant or controllable due to the unpredictability of the solids migration and effluent spikes. The SRT proposed by Hahn et al (2015) was on the order of 23-65 days, which brings into question the accuracy of using SRT in this system without wasting.

CHAPTER 5

CONCLUDING REMARKS AND FUTURE RECOMMENDATIONS

5.1 Conclusion

An understanding of the dominant functions impacting the microbial degradation of substrate in an ABR is required for modeling. Two years of performance data were analyzed using only three model substrates to develop stoichiometries and pseudo first order kinetics to describe the microbial functions of hydrolysis, fermentation, and methanogenesis.

Evaluation of the mass balance identified a major gap in Cell 1, indicating that the assumption that particulate COD was removed by grease and hydrolysis alone was not sufficient. The addition of a pCOD gravitational settling sink to Cell 1 allowed for the mass balance to close within 8%. With this added sink in Cell 1, the eight assumed major sources and sinks of COD were representative of the ABR based on mass balance closure. The mass balance results were good considering the ABR is a biological system receiving diurnally variable influent composition.

The gravitational settling function was attributed to Cell 1 alone due to its pCOD removal capabilities being far greater than the downstream Cells. Cell 4 showed an increase in pCOD over the course of the two years pointing to a solids migration function occurring in the Cells. The solids travel between cells over time was not related to temperature or flowrate.

The pCOD (“cellulose”) removal model was improved when pCOD gravitational settling was incorporated in Cell 1. The subsequent overall model worked well to predict effluent $pCOD_{\text{cellulose}}$ and $dCOD_{\text{glucose}}$ concentrations across all Cells. MLVSS was not a good proxy for active biomass, which in part can be attributed to the lack of a constant or quantifiable mean cell

resident time (MCRT) which not equivalent to SRT in a system receiving influent particulate matter. Such analysis can provide a framework to better inform anaerobic reactor design and understanding.

5.2 Recommendations

The investigation of the pilot-scale ABR led to a few recommendations that will assist in future research efforts. First of all, there exists a solids migration function that was not accounted for in the kinetic analysis, though the model developed was able to describe the COD exiting each Cell. In order to understand this phenomenon, core data needs to be analyzed more frequently to fully capture the effects of solids migration. In order to mitigate the solids migration effect, the storage capacity of the ABR Cells should be determined in order to develop a periodic solid wasting strategy that could eliminate the unpredictable solids movement between Cells.

Second, particulate COD played a strong role in analyzing this ABR fed a raw wastewater substrate. It was assumed that all pCOD entering the ABR was biodegradable; however, there was an increase in average pCOD observed in Cell 4, shown in Table 4.2. The inclusion of stoichiometric microbial biomass production may account for some of the observed increases in particulate COD concentrations observed in Cell 4, and could help to close the mass balance completely in the other Cells.

Finally, teasing out the active microbial biomass within each Cell did not work as hypothesized. MLVSS is not a good proxy for active biomass in anaerobic systems, and solids residence time (SRT) is not the same as mean cell residence time (MCRT). A better representation of active microorganisms in an anaerobic system is needed.

REFERENCES CITED

- Adekunle, K. F., & Okolie, J. A. (2015). A Review of Biochemical Process of Anaerobic Digestion. *Advances in Bioscience and Biotechnology*, 6(3), 205–212. <https://doi.org/10.4236/abb.2015.63020>
- Álvarez, J. A., Armstrong, E., Gómez, M., & Soto, M. (2008). Anaerobic treatment of low-strength municipal wastewater by a two-stage pilot plant under psychrophilic conditions. *Bioresource Technology*, 99(15), 7051–7062. <https://doi.org/10.1016/j.biortech.2008.01.013>
- American Public Health Association (APHA), American Water Works Association, & Water Environment Federation. (2005). *Standard Methods for the Examination of Water and Wastewater 21st Edition. Standard Methods*.
- Bachmann, A., & Beard, V. L. (1985). P E R F O R M A N C E CHARACTERISTICS OF THE ANAEROBIC BAFFLED REACTOR, 19(1), 99–106.
- Bachmann, A., Beard, V. L., & McCarty, P. L. (1982). Bachman et al 1982 fixed film ABR.pdf. Kings Island, Ohio: First International Conference on Fixed-Film Biological Processes.
- Barber, W. P., & Stuckey, D. C. (1999). Review Paper (Abr) for Wastewater Treatment : a Review, 33(7).
- Batstone, D. J., Keller, J., Angelidaki, I., Kalyuzhnyi, S. V., Pavlostathis, S. G., Rozzi, A., ... Vavilin, V. A. (2002). The IWA Anaerobic Digestion Model No 1 (ADM1). *Water Science and Technology*, 45(10), 65–73. <https://doi.org/10.2166/wst.2008.678>
- Batstone, D. J., Keller, J., Newell, R. B., & Newland, M. (2000). Modelling anaerobic degradation of complex wastewater. II: Parameter estimation and validation using slaughterhouse effluent. *Bioresource Technology*, 75(1), 75–85. [https://doi.org/10.1016/S0960-8524\(00\)00019-5](https://doi.org/10.1016/S0960-8524(00)00019-5)
- Beguin, P., & Aubert, J.-P. (1994). The biological degradation of cellulose. *FEMS Microbiology Reviews*, 13(1), 25–58. <https://doi.org/10.1111/j.1574-6976.1994.tb00033.x>
- Bryant, M. P. (1979). Microbial methane production – Theoretical aspects. *Journal of Animal Scienceof*, 48, 193–201. <https://doi.org/10.2134/jas1979.481193x>
- Ellis, T. G. (2004). Chemistry of Wastewater (Vol II). Encyclopedia of Life Support Systems.
- Fulton, L., Mangelsdorff, A. D., & Finstuen, K. (2008). Using Anscombe’s Quartet Plus One To Illustrate Data Set Matching, Proper Model Specification, And Relationships Between Inferential Tests. *J Health Adm Educ*, 25(2), 145–158.
- Guest, J. S., Skerlos, S. J., Barnard, J. L., Beck, M. B., Daigger, G. T., Hilger, H., ... Love, N. G. (2009). A new planning and design paradigm to achieve sustainable resource recovery from wastewater. *Environmental Science and Technology*, 43(16), 6126–6130.

<https://doi.org/10.1021/es9010515>

- Hahn, M. J., & Figueroa, L. A. (2015). Pilot scale application of anaerobic baffled reactor for biologically enhanced primary treatment of raw municipal wastewater. *Water Research*, 87, 494–502. <https://doi.org/10.1016/j.watres.2015.09.027>
- Hahn, M. J., & Figueroa, L. A. (2016). Anaerobic baffled reactor pilot : bridging the gap to energy positive wastewater treatment. Retrieved from <https://dspace.library.colostate.edu/handle/11124/170600>
- Hemsi, P. S., Shackelford, C. D., & Figueroa, L. A. (2010). Calibration of Reactive Transport Models for Remediation of Mine Drainage in Solid-Substrate Biocolumns. *Journal of Environmental Engineering-Asce*, 136(9), 914–925. [https://doi.org/10.1061/\(asce\)ee.1943-7870.0000234](https://doi.org/10.1061/(asce)ee.1943-7870.0000234)
- Henze, M., Gujer, W., Mino, T., & van Loosedrecht, M. (2015). Activated Sludge Models ASM1, ASM2, ASM2d and ASM3. *Water Intelligence Online*, 5(0), 9781780402369–9781780402369. <https://doi.org/10.2166/9781780402369>
- Kaspar, H. F., & Wuhrmann, K. (1978). Kinetic parameters and relative turnovers of some important catabolic reactions in digesting sludge. *Applied and Environmental Microbiology*, 36(1), 1–7.
- La Motta, E. J., Padrón, H., Silva, E., Luque, J., Bustillos, A., & Corzo, P. (2008). Pilot Plant Comparison between the AFBR and the UASB Reactor for Municipal Wastewater Pretreatment. *Journal of Environmental Engineering*, 134(4), 265–272. [https://doi.org/10.1061/\(ASCE\)0733-9372\(2008\)134:4\(265\)](https://doi.org/10.1061/(ASCE)0733-9372(2008)134:4(265))
- Lettinga, G., Hobma, S. W., & Hulshoff Pol, L. W. (1983). Design operation and economy of anaerobic treatment. *Water Science and Technology*, 15(8–9), 177–195.
- Lettinga, G., & Hulshoff Pol, L. (1991). UASB-Process design for various types of wastewates. *Water Science and Technology*, 24(8), 87–107.
- Li, J., Shi, E., Antwi, P., & Leu, S.-Y. (2016). Modeling the performance of an anaerobic baffled reactor with the variation of hydraulic retention time. *Bioresourc Technology*, 214, 477–486. <https://doi.org/10.1016/j.biortech.2016.04.128>
- McCarty, P. L. (1964). Anaerobic Waste Treatment Fundamentals. *Chemistry and Microbiology*, 95(9), 107–112. https://doi.org/10.1300/J118v09n01_08
- McCarty, P. L., Bae, J., & Kim, J. (2011). Domestic wastewater treatment as a net energy producer-can this be achieved? *Environmental Science and Technology*, 45(17), 7100–7106. <https://doi.org/10.1021/es2014264>
- McCarty, P. L., & Mosey, F. (1991). Modelling of anaerobic digestion process - a discussion of concepts. *Water Science Technology*, 24(8), 17–33.

- Merlin Christy, P., Gopinath, L. R., & Divya, D. (2014). A review on anaerobic decomposition and enhancement of biogas production through enzymes and microorganisms. *Renewable and Sustainable Energy Reviews*, 34, 167–173. <https://doi.org/10.1016/j.rser.2014.03.010>
- Mizuta, K., & Shimada, M. (2010). Benchmarking energy consumption in municipal wastewater treatment plants in Japan. *Water Science and Technology*, 62(10), 2256–2262. <https://doi.org/10.2166/wst.2010.510>
- Mosey, F. E. (1983). Mathematical modelling of the anaerobic digestion process: Regulatory mechanisms for the formation of short-chain volatile acids from glucose. *Water Science and Technology*, 15(8–9), 209–232.
- Nachaiyasit, S., & Stuckey, D. C. (1995). Microbial response to environmental changes in an Anaerobic Baffled Reactor (ABR). *Antonie van Leeuwenhoek*, 67(1), 111–23. Retrieved from <http://www.ncbi.nlm.nih.gov/pubmed/7741525>
- Pavlostathis, S. G., & Giraldo-Gomez, E. (1991). Kinetics of anaerobic treatment. In *Water Science and Technology* (Vol. 24, pp. 35–59).
- Rittmann, B. E., & McCarty, P. L. (2001). *Environmental Biotechnology: Principles and Applications. Biotechnology*. Retrieved from <http://books.google.com/books?id=S6CiK7Nh9oIC&printsec=frontcover>
- Shoener, B. D., Bradley, I. M., Cusick, R. D., & Guest, J. S. (2014). Energy positive domestic wastewater treatment: the roles of anaerobic and phototrophic technologies. *Environ. Sci.: Processes Impacts*, 16(6), 1204–1222. <https://doi.org/10.1039/C3EM00711A>
- Skiadas, I. V., Gavala, H. N., & Lyberatos, G. (2000). Modelling of the periodic anaerobic baffled reactor (PABR) based on the retaining factor concept. *Water Research*, 34(15), 3725–3736. [https://doi.org/10.1016/S0043-1354\(00\)00137-8](https://doi.org/10.1016/S0043-1354(00)00137-8)
- Skiadas, I. V., & Lyberatos, G. (1998). The periodic anaerobic baffled reactor. In *Water Science and Technology* (Vol. 38, pp. 401–408). [https://doi.org/10.1016/S0273-1223\(98\)00717-3](https://doi.org/10.1016/S0273-1223(98)00717-3)
- Stamatelatou, K., & Lyberatos, G. (2002). Simulation of a periodic anaerobic baffled reactor (PABR): steady state and dynamic response. *Water Science and Technology*, 45(10), 81–86.
- Stamatelatou, K., Vavilin, V., & Lyberatos, G. (2003). Performance of a glucose fed periodic anaerobic baffled reactor under increasing organic loading conditions: 1. Experimental results. *Bioresource Technology*, 88(2), 131–136. [https://doi.org/10.1016/S0960-8524\(02\)00276-6](https://doi.org/10.1016/S0960-8524(02)00276-6)
- Tchobanoglous, G., Burton, F. L., & Stensel, H. D. (2014). *Wastewater Engineering: Treatment and Resource Recovery. Metcalf & Eddy*. [https://doi.org/10.1016/0309-1708\(80\)90067-6](https://doi.org/10.1016/0309-1708(80)90067-6)
- Vavilin, V. a. (1996). A description of hydrolysis kinetics in anaerobic degradation of particulate organic matter. *Science*, 56, 229–237.

- Vavilin, V. A., Vasiliev, V. B., Ponomarev, A. V., & Rytov, S. V. (1994). Simulation model “methane” as a tool for effective biogas production during anaerobic conversion of complex organic matter. *Bioresource Technology*, 48(1), 1–8. [https://doi.org/10.1016/0960-8524\(94\)90126-0](https://doi.org/10.1016/0960-8524(94)90126-0)
- Vavilin, V. A., Vasiliev, V. B., & Rytov, S. V. (1996). Simulation of constituent processes of anaerobic degradation of organic matter by the <methane> model. *Antonie van Leeuwenhoek, International Journal of General and Molecular Microbiology*, 69(1), 15–23. <https://doi.org/10.1007/BF00641607>
- Wang, J., Huang, Y., & Zhao, X. (2004). Performance and characteristics of an anaerobic baffled reactor. *Bioresource Technology*, 93(2), 205–208. <https://doi.org/10.1016/j.biortech.2003.06.004>
- Wyman, C., Decker, S., Himmel, M., Brady, J., Skopec, C., & Viikari, L. (2004). *Hydrolysis of Cellulose and Hemicellulose. Polysaccharides*. <https://doi.org/10.1201/9781420030822.ch43>
- Xing, J., Bgopathy, R., & Tilche, A. (1991). Model evaluation of hybrid anaerobic baffled reactor treating molasses wastewater. *Biomass and Bioenergy*, 1(5), 267–274. [https://doi.org/10.1016/0961-9534\(91\)90038-E](https://doi.org/10.1016/0961-9534(91)90038-E)
- Xing, J., & Tilche, A. (1992). The effect of hydraulic retention time on the hybrid anaerobic baffled reactor performance at constant loading. *Biomass and Bioenergy*, 3(1), 25–29. [https://doi.org/10.1016/0961-9534\(92\)90016-J](https://doi.org/10.1016/0961-9534(92)90016-J)
- Ye, Z., & Berson, R. E. (2011). Kinetic modeling of cellulose hydrolysis with first order inactivation of adsorbed cellulase. *Bioresource Technology*, 102(24), 11194–11199. <https://doi.org/10.1016/j.biortech.2011.09.044>
- Yu, L., & Wensel, P. C. (2013). Mathematical Modeling in Anaerobic Digestion (AD). *Journal of Bioremediation & Biodegradation*, s4. <https://doi.org/10.4172/2155-6199.S4-003>

APPENDIX A

METHANE CALCULATIONS

The amount of methane and dissolved methane in each of the cells was calculated using the following method.

A.1 Biogas Flowrate

The biogas flowrate was measured for each of the cells over the course of August 2012 to July 2014. A monthly average of the biogas flowrate was calculated for each cell.

Table A.1: Biogas flowrate measurements over time.

Date	Biogas Flowrate mL/min Measurements				
Mo.-Yr.	Cell 1	Cell 2	Cell 3	Cell 4	Total
Aug-12	10.69	31.84	24.95	42.59	110.07
Sep-12	8.68	28.37	24.36	45.18	106.59
Oct-12	12.39	23.84	19.74	36.54	92.51
Nov-12	13.59	24.73	22.23	47.74	108.29
Dec-12	16.88	19.99	40.96	41.61	119.44
Jan-13	17.38	15.11	26.3	40.69	99.48
Feb-13	16.23	17.43	26.25	36.87	96.78
Mar-13	16.75	16.04	17.68	30.00	80.47
Apr-13	10.9	14.6	14.6	18.37	58.47
May-13	7.89	18.05	6.96	17.02	49.92
Jun-13	8.16	17.59	24.21	22.51	72.47
Jul-13	9.9	23.85	22.17	31.61	87.53
Aug-13	10.69	31.84	24.95	42.59	110.07
Sep-13	15.81	22.92	24.36	47.76	110.85
Oct-13	26.7	23.84	21.85	54.19	126.58
Nov-13	26.31	24.73	28.87	43.9	123.81
Dec-13	26.67	19.63	40.96	39.74	127
Jan-14	27.31	25.74	26.3	40.69	120.04
Feb-14	22.53	25.53	20.26	33.19	101.51
Mar-14	18.14	19.49	9.65	29.04	76.32
Apr-14	11.83	14.64	14.6	16.77	57.84
May-14	6.96	20.68	6.84	35.62	70.1
Jun-14	15.28	25.29	24.21	38.22	103
Jul-14	12.8	27.17	25.74	40.41	106.12

The total measured biogas flowrate was compared to the calculated total biogas flowrate using the following equation seen in Hahn and Figueroa, 2015.

$$\text{Biogas Flowrate (mL/min)} = 117 * 1.09^{(\text{Temperature influent} - 19.7)}$$

The temperature used is a monthly average of the influent temperature data, consistent with the methods of Hahn and Figueroa, 2015.

Table A.2: Calculated biogas concentration based on temperature, over time. Percent difference is calculated for the measured total biogas flowrate versus the calculated biogas flowrate.

Date	Temperature C	Measured Biogas Flowrate mL/min	Calculated Biogas Flowrate mL/min	% Difference
Mo.-Yr.	Influent Average	C1+C2+C3+C4	$= 117 * 1.09^{(T_{\text{influent}} - 19.7)}$	$= (\text{Measured} - \text{Calculated}) / \text{Measured} * 100\%$
Aug-12	21.8	110.07	140.8	-27.9%
Sep-12	21.9	106.59	141.8	-33.0%
Oct-12	20.7	92.51	127.3	-37.6%
Nov-12	19.0	108.29	110.5	-2.0%
Dec-12	17.3	119.44	95.2	20.3%
Jan-13	15.6	99.48	82.1	17.5%
Feb-13	14.7	96.78	76.1	21.4%
Mar-13	14.4	80.47	74.2	7.8%
Apr-13	15.1	58.47	78.4	-34.1%
May-13	16.3	49.92	87.0	-74.3%
Jun-13	17.3	72.47	95.3	-31.5%
Jul-13	20.2	87.53	121.8	-39.2%
Aug-13	21.2	110.07	132.7	-20.6%
Sep-13	21.2	110.85	133.5	-20.4%
Oct-13	20.2	126.58	121.7	3.9%
Nov-13	18.6	123.81	106.5	14.0%
Dec-13	16.7	127	90.3	28.9%
Jan-14	15.3	120.04	80.0	33.4%
Feb-14	14.4	101.51	73.9	27.2%
Mar-14	14.5	76.32	74.5	2.4%
Apr-14	15.2	57.84	79.3	-37.1%
May-14	16.4	70.1	87.8	-25.2%
Jun-14	18.0	103	100.7	2.2%
Jul-14	19.7	106.12	116.7	-10.0%

Due to the variability in the percent difference between the measured flowrate and the modeled flowrate, it was decided that the measurements would be used for the remainder of the methane analysis.

A.2 Measured Biogas Flowrate at Ambient Temperature to Biogas Flowrate at STP

The measured biogas flowrate was at ambient temperature and pressure. The ambient temperatures can be assumed to be the influent wastewater temperature as it is an anaerobic system, and as used in the previous section. The ambient pressure is 0.81 in Castle Rock, CO at an elevation of 6,224 ft. Using the ideal gas law, the ambient biogas flowrate can be converted to the flowrate at STP.

$$P*V=n*R*T$$

Where P = 0.81 atm, V = 22.4 L, n = 1 mol, R = 0.08205736 L*atm*mol⁻¹*K⁻¹, T = 273.15 K + Influent Temperature (C).

Table A.3: Total measured biogas flowrate at standard temperature and pressure over time.

Date	Temperature C	Measured Biogas Flowrate (Ambient) mL/min	Measured Biogas Flowrate (STP) L/day
Mo.-Yr.	Influent Monthly Average	C1+C2+C3+C4	C1+C2+C3+C4
Aug-12	21.8	110.07	118.80
Sep-12	21.9	106.59	115.01
Oct-12	20.7	92.51	100.25
Nov-12	19.0	108.29	118.01
Dec-12	17.3	119.44	130.93
Jan-13	15.6	99.48	109.70
Feb-13	14.7	96.78	107.05

Table A.3 Continued.

Mar-13	14.4	80.47	89.10
Apr-13	15.1	58.47	64.60
May-13	16.3	49.92	54.92
Jun-13	17.3	72.47	79.44
Jul-13	20.2	87.53	95.02
Aug-13	21.2	110.07	119.08
Sep-13	21.2	110.85	119.89
Oct-13	20.2	126.58	137.41
Nov-13	18.6	123.81	135.12
Dec-13	16.7	127	139.52
Jan-14	15.3	120.04	132.51
Feb-14	14.4	101.51	112.42
Mar-14	14.5	76.32	84.49
Apr-14	15.2	57.84	63.87
May-14	16.4	70.1	77.09
Jun-14	18.0	103	112.66
Jul-14	19.7	106.12	115.39

This method was followed in order to determine the biogas flowrate at STP for each of the four cells as well.

Table A.4: Measured biogas flowrate at standard temperature and pressure for Cells 1-4 over time.

Date	Measured Biogas Flowrate (STP) L/day			
Mo.-Yr.	Cell 1	Cell 2	Cell 3	Cell 4
Aug-12	11.54	34.37	26.93	45.97
Sep-12	9.37	30.61	26.29	48.75
Oct-12	13.43	25.83	21.39	39.60
Nov-12	14.81	26.95	24.22	52.02
Dec-12	18.50	21.91	44.90	45.61
Jan-13	19.17	16.66	29.00	44.87
Feb-13	17.95	19.28	29.04	40.78
Mar-13	18.55	17.76	19.58	33.22
Apr-13	12.04	16.13	16.13	20.30
May-13	8.68	19.86	7.66	18.72
Jun-13	8.94	19.28	26.54	24.67
Jul-13	10.75	25.89	24.07	34.31
Aug-13	11.56	34.45	26.99	46.08
Sep-13	17.10	24.79	26.35	51.66
Oct-13	28.98	25.88	23.72	58.83
Nov-13	28.71	26.99	31.51	47.91
Dec-13	29.30	21.56	45.00	43.66
Jan-14	30.15	28.41	29.03	44.92
Feb-14	24.95	28.27	22.44	36.76
Mar-14	20.08	21.58	10.68	32.15
Apr-14	13.06	16.17	16.12	18.52
May-14	7.65	22.74	7.52	39.17
Jun-14	16.71	27.66	26.48	41.80
Jul-14	13.92	29.54	27.99	43.94

A.3 Percent Methane in the Biogas

The percentage of biogas that is methane was found using a Shimadzu Gas Chromatograph. Gas samples were collected from the headspace of each of the four ABR cells in gas collection bags. The gas samples were stored at room temperature until their analysis in the GC machine. The Shimadzu Gas Chromatograph used a helium carrier gas and a thermal conductivity detector was used for CH₄, CO₂, and N₂ analyses. A Hamilton gas tight syringe was used to manually inject standards and samples into the GC. Calibration standards bracketing the samples' gas concentrations were run each day. The calibration curve was calculated by the peak area and moles as calculated by the ideal gas law, $PV=nRT$, at ambient temperature and pressure, with the given injection volume. These results were in the form of $y=mx+b$, where y is the μmol , and x is the area of the sample.

Biogas samples from June 2013 to August 2014 were analyzed for their biogas composition, and an average percent methane in the biogas was used to obtain the methane flowrate in L/day.

Table A.5: Percent methane in the biogas for Cells 1-4 over time.

Date	% CH ₄ in Biogas			
	Cell 1	Cell 2	Cell 3	Cell 4
6/19/13	43%	87%	87%	76%
6/20/13	52%	77%	81%	81%
7/3/13	43%	75%	75%	80%
7/12/13	54%	65%	66%	73%
4/12/14		68%	68%	73%
4/12/14		62%		
4/12/14		67%	66%	74%
4/16/14	52%	69%	72%	76%
5/7/14	49%	53%	64%	74%
5/21/14	57%	60%	66%	76%
6/9/14	65%	75%	78%	85%
6/9/14	66%	76%	79%	85%
6/29/14	58%	83%	83%	91%
7/14/14				70%
7/15/14	63%	75%	83%	89%
7/21/14	59%	68%	75%	82%

Table A.5 Continued.

7/21/14	59%	75%	81%	91%
7/24/14				78%
7/24/14				84%
7/28/14				83%
7/29/14	62%	70%	81%	85%
7/28/14				84%
7/31/14				84%
Average	55%	72%	75%	81%
Standard Deviation	7.9%	8.2%	7.8%	5.9%

The average percent methane in the biogas was multiplied by the measured biogas flowrate at STP in order to determine the methane flowrate for each cell.

Table A.6: Methane flowrate at standard temperature and pressure for Cells 1-4 over time.

Date	Methane Flowrate (STP) L/day			
	Cell 1	Cell 2	Cell 3	Cell 4
Aug-12	6.29	24.83	20.22	37.01
Sep-12	5.11	22.12	19.74	39.25
Oct-12	7.32	18.67	16.06	31.88
Nov-12	8.08	19.47	18.19	41.89
Dec-12	10.09	15.83	33.71	36.73
Jan-13	10.45	12.04	21.77	36.13
Feb-13	9.79	13.93	21.80	32.84
Mar-13	10.11	12.83	14.70	26.75
Apr-13	6.57	11.66	12.11	16.34
May-13	4.73	14.35	5.75	15.08
Jun-13	4.88	13.93	19.92	19.87
Jul-13	5.86	18.71	18.07	27.63
Aug-13	6.31	24.89	20.27	37.10
Sep-13	9.32	17.91	19.78	41.59
Oct-13	15.81	18.70	17.81	47.37
Nov-13	15.66	19.50	23.65	38.58
Dec-13	15.98	15.58	33.78	35.15
Jan-14	16.44	20.53	21.80	36.17
Feb-14	13.61	20.43	16.85	29.60
Mar-14	10.95	15.59	8.02	25.89
Apr-14	7.12	11.68	12.10	14.91
May-14	4.17	16.43	5.65	31.54
Jun-14	9.11	19.99	19.88	33.66
Jul-14	7.59	21.35	21.01	35.38

A.4 Dissolved Methane Concentration

The Dissolved Methane Concentration of the sample was calculated using Henry's constant (k_{Hi}), the percent methane in the headspace above the liquid of the ABR (found in the previous section, % CH₄), and ambient pressure (P_1).

$$(DMC_{ABR}) = \% CH_4 * P_1 * k_{Hi}$$

A.4.1 Oversaturation Calculation

Approximately 1.18 g BESA was added to 250 mL serum bottles (~20mM). ABR effluent was collected directly into the serum bottle leaving a small headspace, and the bottle was immediately sealed with a septum and aluminum cap. Initially, a second sample was prepared without BESA, for comparison. Bottles were weighed to determine the headspace volume. The Shimadzu Gas Chromatograph was used for the headspace composition analysis. The gas analysis was conducted in the same manner as was done for the ABR biogas samples.

After 24 hours at ambient temperature, the headspace concentration of the serum bottle (%CH_{4S}) was used to calculate the dissolved methane concentration in the liquid in the serum bottle (DMC_S). However, as oversaturated gases were coming out of solution, the pressure and the molar concentration of gas in the bottle were expected to increase. The pressure in the serum bottle after 24 hours was calculated by:

$$P_2 = n_2 * P_1 / n_1$$

$$n_1 = P_1 V_{hs} / RT_2$$

Where $P_1 = 0.81$ Ambient Pressure (atm), $P_2 =$ Pressure in Serum Bottle after 24 hours (atm),
 $V_{hs} =$ Volume of Headspace of Serum Bottle (L), $V_i =$ Volume Injected into GC (L), $T_2 =$ ambient
(K), $R = 0.0821$ L*atm/mol*K, $n_1 = P_1 V_{hs} / RT_2$, $n_2 = (P_1 V_{hs} / RT_2) + (\text{moles CH}_4 + \text{moles CO}_2) * V_{hs} / V_i$

The serum headspace concentration (%CH_{4S}) was calculated by two methods:

1. Moles CH_{4S} measured/ expected mol per V_i
2. Moles CH_{4S} measured/ (Moles N₂ measured + Moles CH₄ measured + Moles CO₂ measured)

Method 2 resulted in more consistent results, however neglects oxygen in headspace of serum bottle.

The final moles in the serum bottle after equilibration were the sum of the serum bottle dissolved methane and the serum bottle headspace.

$$\text{Final Moles in Serum Bottle} = C_S * V_{hs} + DMC_S * V_{liq}$$

Where $C_S =$ Moles CH₄ measured in serum headspace/Sample Volume (mol/L) and $V_{liq} =$ Volume of Liquid in Serum Bottle (L).

Oversaturation was calculated as (Final-Expected)/Final.

$$((DMC_S * V_{liq} + C_S * V_{hs}) - (DMC_{ABR} * V_{liq})) / (DMC_{ABR} * V_{liq})$$

A.4.2) Henry's Constant Adjustment

The Henry's law constant was adjusted for ambient temperature according the formula:

$$K_h = k_{Hi} * \exp((\Delta H_{sol}/R) * (1/T_2 - 1/T_1))$$

Where $\Delta H_{sol}=1600$, $k_{Hi}=0.001305 \text{ mol/L*atm}$, and $T_1=298.15 \text{ K}$.

A.4.3 Total Dissolved Methane Concentration at Ambient and STP

After the oversaturation and Henry's constant adjustment were made, obtaining the L/day of dissolved methane was relatively straightforward with the following calculation:

$$DMC_{Ambient} \text{ (L/day)} = (K_h * Q * P_1) / \text{oversaturation}$$

Where Q is 1728 L/day, the flowrate of the ABR system. From there, using the ideal gas law, the dissolved methane concentration at STP was obtained.

$$DMC_{STP} \text{ (L/day)} = (DMC_{Ambient} * V * P_1) / (n * R * T_2)$$

Table A.7: Henry's constant (Kh) used to determine the dissolved methane concentration (DMC) at standard temperature and pressure from the ambient measurements, over time.

Date	K_h	$DMC_{Ambient}$ (L/day)	DMC_{STP} (L/day)
Aug-12	29.89	62.28	46.68
Sep-12	29.93	62.20	46.61
Oct-12	29.37	63.38	47.69
Nov-12	28.64	64.99	49.18
Dec-12	27.89	66.74	50.81
Jan-13	27.15	68.56	52.50
Feb-13	26.78	69.52	53.40
Mar-13	26.65	69.85	53.71
Apr-13	26.92	69.14	53.05

Table A.7 Continued.

May-13	27.44	67.84	51.83
Jun-13	27.90	66.73	50.80
Jul-13	29.14	63.87	48.15
Aug-13	29.59	62.92	47.27
Sep-13	29.62	62.85	47.21
Oct-13	29.14	63.88	48.16
Nov-13	28.46	65.41	49.57
Dec-13	27.62	67.39	51.41
Jan-14	27.02	68.89	52.81
Feb-14	26.63	69.90	53.76
Mar-14	26.67	69.79	53.65
Apr-14	26.98	68.99	52.91
May-14	27.49	67.72	51.72
Jun-14	28.18	66.07	50.18
Jul-14	28.92	64.36	48.60

A.5 Percent Dissolved Methane

The percent dissolved methane was calculated using the DMC_{STP} divided by the total (Sum of cells 1 – 4) methane flowrate plus the DMC_{STP} . The percentage obtained was then used to estimate the dissolved methane concentration in each of the four cells.

Table A.8: Percent dissolved methane concentration found from the DMC at standard temperature and pressure divided by the total methane flowrate at standard temperature and pressure, over time.

Date	DMC_{STP} (L/day)	Total Methane Flowrate (STP) L/day	Percent DMC (%)
		C1+C2+C3+C4	$(DMC_{STP}) / (Total\ Methane\ Flowrate\ STP + DMC_{STP})$
Aug-12	46.68	118.80	28.21%
Sep-12	46.61	115.01	28.84%
Oct-12	47.69	100.25	32.24%
Nov-12	49.18	118.01	29.42%
Dec-12	50.81	130.93	27.96%
Jan-13	52.50	109.70	32.37%
Feb-13	53.40	107.05	33.28%
Mar-13	53.71	89.10	37.61%
Apr-13	53.05	64.60	45.09%
May-13	51.83	54.92	48.55%

Table A.8 Continued.

Jun-13	50.80	79.44	39.00%
Jul-13	48.15	95.02	33.63%
Aug-13	47.27	119.08	28.42%
Sep-13	47.21	119.89	28.25%
Oct-13	48.16	137.41	25.95%
Nov-13	49.57	135.12	26.84%
Dec-13	51.41	139.52	26.93%
Jan-14	52.81	132.51	28.50%
Feb-14	53.76	112.42	32.35%
Mar-14	53.65	84.49	38.84%
Apr-14	52.91	63.87	45.31%
May-14	51.72	77.09	40.15%
Jun-14	50.18	112.66	30.82%
Jul-14	48.60	115.39	29.64%

APPENDIX B

MODEL INPUTS AND FITTING PARAMETERS

The mass balance was analyzed using actual concentrations of particulate, dissolved, and gaseous substrate entering each Cell of the ABR. The K values were derived using the actual concentrations. Modelled effluent $p\text{COD}_{\text{cellulose}}$ and $d\text{COD}_{\text{glucose}}$ concentrations were predicted using actual influent concentrations and K values.

B.1 Actual COD Concentrations and Cell 1 $p\text{COD}_{\text{settled}}$ Sink

The actual COD concentrations that were used to determine the mass balance closure and the mass balance ratio of $\text{COD}_{\text{out}} : \text{COD}_{\text{in}}$ that was used to determine the $p\text{COD}_{\text{settled}}$ concentration are shown in the following section.

B.1.1 Actual COD Concentrations

Influent actual concentrations that were used in the mass balance, determining K values, and also the influent values for the model simulation are shown in Table B.1 below.

Table B.1: Influent concentrations of $p\text{COD}_{\text{cellulose}}$, $d\text{COD}_{\text{glucose}}$, and $d\text{COD}_{\text{acetate}}$ in units of mg COD/L. Note that the influent concentrations for methane and dissolved methane are zero.

Date	$p\text{COD}_{\text{cellulose}}$	$d\text{COD}_{\text{glucose}}$	$d\text{COD}_{\text{acetate}}$
Aug-12	565.8	139.3	48.9
Sep-12	448.2	117.5	51.9
Oct-12	531.7	168.8	22.1
Nov-12	554.6	163.8	26.7
Dec-12	502.2	164.5	31.3
Jan-13	573.3	194.9	7.8
Feb-13	604.9	163.7	28.1
Mar-13	522.2	175.0	32.8

Table B.1 Continued.

Apr-13	526.8	164.2	32.0
May-13	547.3	134.8	28.0
Jun-13	581.7	144.5	31.1
Jul-13	548.7	119.3	32.4
Aug-13	505.6	146.7	50.3
Sep-13	501.5	108.2	52.5
Oct-13	613.6	127.2	21.0
Nov-13	845.5	131.9	22.4
Dec-13	832.3	131.6	24.2
Jan-14	477.0	105.4	41.0
Feb-14	514.3	141.8	31.2
Mar-14	683.7	111.6	18.1
Apr-14	628.2	114.0	22.6
May-14	530.8	110.0	23.2
Jun-14	568.0	102.5	21.5
Jul-14	794.5	105.3	24.2

The influent concentrations were used in both the mass balance, and were the input concentrations used in the modeling of the ABR. The actual measured concentrations for Cell 1 are shown in Table B.2 below.

Table B.2: Average monthly experimentally determined data for Cell 1 in units of g COD/L. Note that pCOD consists of pCOD_{cellulose} and pCOD_{grease}.

Date	pCOD_{cellulose} + pCOD_{grease}	dCOD_{glucose} + dCOD_{SRB}	gCOD_{CH4}	dCOD_{CH4}	dCOD_{acetate}
Aug-12	172.4	155.6	6.6	1.9	98.3
Sep-12	217.2	156.7	5.4	1.4	65.7
Oct-12	159.8	192.1	7.7	2.1	67.8
Nov-12	213.5	179.1	8.5	2.0	66.9
Dec-12	252.9	175.7	10.6	4.1	56.3
Jan-13	212.1	272.5	11.0	3.4	
Feb-13	284.1	241.6	10.3	3.4	54.9
Mar-13	230.3	191.3	10.7	3.2	75.4
Apr-13	228.8	188.8	6.9	2.6	87.8
May-13	226.0	173.4	5.0	1.2	70.1
Jun-13	217.2	143.4	5.1	2.3	85.4
Jul-13	306.7	129.5	6.2	2.0	82.0
Aug-13	121.0	193.4	6.7	1.9	75.3
Sep-13	274.6	125.4	9.8	2.5	61.8
Oct-13	229.6	133.6	16.7	3.4	51.5
Nov-13	246.6	145.9	16.5	4.9	43.2
Dec-13	204.1	155.5	16.9	6.7	46.6
Jan-14	181.7	162.4	17.3	5.1	47.4

Table B.2 Continued.

Feb-14	229.6	178.3	14.4	4.2	28.6
Mar-14	255.6	166.9	11.6	2.3	39.1
Apr-14	202.0	142.1	7.5	3.0	33.2
May-14	194.1	180.2	4.4	0.5	20.9
Jun-14	209.5	160.4	9.6	2.9	17.7
Jul-14	297.9	152.0	8.0	2.4	33.4

For Cell 1 alone, $dCOD_{\text{glucose}}$ had a $dCOD_{\text{SRB}}$ component attributed to consumed $dCOD$.

The actual measured concentrations for Cell 2 are shown in Table B.3 below.

Table B.3: Average monthly experimentally determined data for Cell 2 in units of g COD/L.

Date	pCOD_{cellulose}	dCOD_{glucose}	gCOD_{CH4}	dCOD_{CH4}	dCOD_{acetate}
Aug-12	112.0	151.7	18.7	5.2	105.3
Sep-12	190.3	139.4	16.6	4.4	102.8
Oct-12	123.3	186.4	14.5	4.0	60.5
Nov-12	183.0	133.3	15.7	3.7	90.0
Dec-12	214.3	144.0	13.2	5.1	73.0
Jan-13	150.3	248.3	10.3	3.2	
Feb-13	137.9	195.7	12.1	4.0	63.0
Mar-13	144.4	177.2	11.2	3.3	81.2
Apr-13	157.0	155.5	10.1	3.8	83.9
May-13	158.9	130.4	12.2	3.0	87.4
Jun-13	184.7	120.1	11.6	5.1	107.9
Jul-13	174.5	111.5	14.7	4.9	94.9
Aug-13	129.1	138.0	19.0	5.3	82.4
Sep-13	99.6	140.4	13.7	3.5	71.0
Oct-13	211.3	133.3	14.7	3.0	52.7
Nov-13	221.9	119.2	15.8	4.7	49.6
Dec-13	181.0	136.4	13.1	5.2	54.1
Jan-14	191.5	156.8	17.7	5.2	37.2
Feb-14	173.2	173.5	17.9	5.2	30.1
Mar-14	256.2	139.0	13.6	2.7	52.0
Apr-14	206.2	162.3	10.1	4.0	35.5
May-14	200.8	159.5	13.9	1.7	26.0
Jun-14	195.6	151.7	16.4	4.9	26.3
Jul-14	196.5	163.2	16.9	5.1	39.3

The actual measured concentrations for Cell 3 are shown in Table B.4 below

Table B.4: Average monthly experimentally determined data for Cell 3 in units of g COD/L.

Date	pCOD _{cellulose}	dCOD _{glucose}	gCOD _{CH4}	dCOD _{CH4}	dCOD _{acetate}
Aug-12	100.1	154.0	16.4	4.6	138.6
Sep-12	130.7	142.8	16.2	4.3	126.0
Oct-12	118.3	153.6	13.6	3.7	114.1
Nov-12	124.1	154.3	14.7	3.5	111.2
Dec-12	174.2	153.6	26.3	10.3	94.8
Jan-13	110.6	251.3	17.8	5.5	56.7
Feb-13	116.4	269.9	17.9	5.9	74.5
Mar-13	145.7	184.3	12.6	3.8	92.5
Apr-13	142.9	155.2	11.1	4.2	94.8
May-13	200.3	130.2	5.4	1.3	91.0
Jun-13	169.4	138.9	17.7	7.8	110.8
Jul-13	198.3	97.2	15.5	5.1	91.2
Aug-13	153.2	134.4	16.4	4.6	85.8
Sep-13	156.6	105.6	16.0	4.0	74.7
Oct-13	183.7	130.6	13.8	2.8	61.0
Nov-13	163.2	122.9	18.3	5.4	49.4
Dec-13	193.5	138.2	25.8	10.2	59.1
Jan-14	176.8	140.1	16.9	5.0	66.3
Feb-14	223.9	169.6	13.6	4.0	33.7
Mar-14	243.5	140.3	7.0	1.4	59.1
Apr-14	198.0	149.2	11.1	4.5	42.2
May-14	177.3	181.8	5.0	0.6	27.7
Jun-14	186.2	157.2	16.2	4.9	31.5
Jul-14	189.9	156.5	17.1	5.1	41.5

The actual measured concentrations for Cell 3 are shown in Table B.4 below

Table B.5: Average monthly experimentally determined data for Cell 4 in units of g COD/L.

Date	pCOD _{cellulose}	dCOD _{glucose}	gCOD _{CH4}	dCOD _{CH4}	dCOD _{acetate}
Aug-12	114.4	170.4	42.1	11.8	123.3
Sep-12	98.8	158.4	44.7	11.9	125.0
Oct-12	157.1	149.3	36.2	9.9	99.4
Nov-12	160.1	144.6	47.3	11.2	97.0
Dec-12	164.1	117.8	41.3	16.1	114.0
Jan-13	160.7	211.7	40.3	12.4	66.1
Feb-13	131.2	243.4	36.6	12.0	79.5
Mar-13	159.9	180.9	29.7	8.9	89.5
Apr-13	195.8	142.1	18.2	6.9	74.3
May-13	187.3	113.4	16.8	4.1	81.9
Jun-13	185.2	135.6	22.3	9.9	67.7
Jul-13	247.2	92.7	31.3	10.4	61.0
Aug-13	197.2	102.8	42.2	11.8	45.6
Sep-13	184.4	95.2	47.3	12.0	47.2
Oct-13	238.1	113.2	53.7	11.0	34.0

Table B.5 Continued.

Nov-13	243.3	99.2	43.5	12.9	35.5
Dec-13	285.4	114.8	39.4	15.6	45.7
Jan-14	227.3	127.4	40.4	11.9	51.6
Feb-14	378.9	143.0	32.9	9.6	28.6
Mar-14	355.0	125.0	28.8	5.6	36.0
Apr-14	277.1	131.0	16.6	6.7	30.4
May-14	284.9	148.0	35.3	4.4	22.3
Jun-14	267.8	126.0	37.9	11.4	19.7
Jul-14	229.4	123.9	40.0	12.0	27.4

B.1.2 Cell 1 pCOD_{settled} Concentrations

The monthly pCOD_{settled} concentrations determined using the COD_{out} : COD_{in} ratio found from the mass balance is shown in Table B.6 below.

Table B.6: The Cell 1 monthly mass balance ratio and the monthly concentration of pCOD attributed to the gravitational settling function in units of g COD/L.

Date	COD_{out} : COD_{in}	pCOD_{settled}
Aug-12	0.6	331.8
Sep-12	0.7	323.6
Oct-12	0.6	321.9
Nov-12	0.6	354.6
Dec-12	0.7	360.9
Jan-13	0.7	374.7
Feb-13	0.8	454.7
Mar-13	0.7	366.3
Apr-13	0.7	377.1
May-13	0.7	372.1
Jun-13	0.6	354.5
Jul-13	0.8	414.7
Aug-13	0.6	291.3
Sep-13	0.7	359.5
Oct-13	0.6	360.5
Nov-13	0.5	407.4
Dec-13	0.5	383.9
Jan-14	0.7	322.8
Feb-14	0.7	344.7
Mar-14	0.6	413.5
Apr-14	0.5	331.5
May-14	0.6	328.7
Jun-14	0.6	339.0
Jul-14	0.6	442.1

B.2 K Values

K values were determined by rearranging Equations 3.13 through 3.15. Equation 3.13 was first rearranged to determine the K_{acetate} value for each Cell. The K_{acetate} bulk kinetic parameter values are shown in Table B.7 below.

Table B.7: Monthly K_{acetate} values determined for each Cell in units of 1/day.

Date	Cell 1	Cell 2	Cell 3	Cell 4
Aug-12	0.61	1.06	-0.12	2.03
Sep-12	0.70	0.95	0.00	2.12
Oct-12	1.00	1.01	-0.04	2.12
Nov-12	0.97	0.63	-0.04	2.80
Dec-12	2.36	0.46	1.80	1.80
Jan-13			1.35	3.60
Feb-13	1.98	0.32	0.86	2.65
Mar-13	1.36	0.08	0.16	1.92
Apr-13	0.96	0.47	0.15	1.20
May-13	0.56	0.66	-0.57	1.12
Jun-13	0.85	0.85	0.80	1.04
Jul-13	0.80	0.97	0.13	2.91
Aug-13	0.79	1.39	-0.23	5.48
Sep-13	1.29	0.47	0.29	5.89
Oct-13	2.16	-0.20	-0.05	8.63
Nov-13	3.67	-0.07	0.56	7.30
Dec-13	4.61	-0.83	2.84	4.14
Jan-14	3.50	0.19	-0.06	4.64
Feb-14	4.75	1.21	-1.10	6.71
Mar-14	1.87	0.29	-0.69	4.02
Apr-14	2.90	0.95	0.35	2.40
May-14	0.84	1.54	-1.26	6.04
Jun-14	5.23	2.59	0.04	11.31
Jul-14	2.30	2.24	0.13	8.64

As shown in Equation 3.13, dissolved methane, gaseous methane, and effluent acetate concentrations were used. Also, gaseous methane flowrate was used from the calculations shown in Appendix A. The monthly K_{acetate} values determined by rearranging Equation 3.13 were used in Equation 3.14 to determine the K_{glucose} values, shown in Table B.8 below.

Table B.8: Monthly K_{glucose} values determined for each Cell in units of 1/day.

Date	Cell 1	Cell 2	Cell 3	Cell 4
Aug-12	3.79	1.44	2.09	0.98
Sep-12	1.30	3.67	1.68	2.11
Oct-12	2.93	0.02	3.58	0.82
Nov-12	2.80	2.34	1.39	1.43
Dec-12	2.46	1.50	2.92	3.96
Jan-13			2.73	1.93
Feb-13	1.74	0.57	0.75	1.34
Mar-13	3.00	0.39	0.74	1.07
Apr-13	3.64	0.07	0.84	-0.68
May-13	2.81	1.94	-0.23	0.22
Jun-13	4.58	2.94	1.05	-2.62
Jul-13	4.63	2.27	-0.24	-0.88
Aug-13	1.74	1.62	0.07	-0.88
Sep-13	1.60	0.98	0.64	0.80
Oct-13	3.45	-0.01	0.63	0.90
Nov-13	2.89	0.51	0.28	1.96
Dec-13	3.30	0.14	1.95	0.94
Jan-14	1.74	-0.62	2.11	1.25
Feb-14	0.84	0.37	-0.06	1.38
Mar-14	1.88	1.10	0.14	-0.41
Apr-14	1.65	0.42	0.59	-0.20
May-14	0.00	0.65	-0.15	0.80
Jun-14	0.51	1.17	0.36	1.34
Jul-14	1.28	1.08	0.19	1.31

The K_{glucose} values were determined based on Equation 3.14 which required the inputs of influent and effluent acetate concentrations, effluent glucose concentrations, and the K_{acetate} values previously shown.

The monthly determined K_{glucose} values were used to determine the $K_{\text{cellulose}}$ values by rearranging Equation 3.15. The $K_{\text{cellulose}}$ values are shown in Table B.9 below.

Table B.9: Monthly $K_{\text{cellulose}}$ values determined for each Cell in units of 1/day.

Date	Cell 1	Cell 2	Cell 3	Cell 4
Aug-12	6.26	2.50	5.12	3.91
Sep-12	3.55	2.95	3.06	6.96
Oct-12	7.02	-0.51	3.66	0.85
Nov-12	4.37	-0.42	4.60	1.22
Dec-12	3.09	-0.25	4.52	1.66

Table B.9 Continued.

Jan-13			9.64	0.87
Feb-13	5.48	-2.76	10.21	1.32
Mar-13	4.59	-0.45	1.99	1.56
Apr-13	5.79	-2.43	1.35	-1.54
May-13	5.27	-0.84	-0.23	-0.88
Jun-13	4.47	1.36	2.62	-3.08
Jul-13	3.33	0.94	-1.03	-0.71
Aug-13	8.77	-2.52	-0.19	-2.60
Sep-13	1.84	3.87	-2.00	-0.06
Oct-13	3.34	-0.02	0.49	-0.23
Nov-13	3.25	-1.02	0.59	0.04
Dec-13	5.16	-1.10	2.20	-0.41
Jan-14	6.08	-1.11	1.38	0.39
Feb-14	2.88	0.22	-0.28	-0.05
Mar-14	4.42	-0.40	0.19	-0.73
Apr-14	3.41	1.66	-0.12	-0.93
May-14	4.31	-0.45	1.27	-0.79
Jun-14	3.88	0.83	0.80	-0.45
Jul-14	2.85	2.03	-0.18	-0.64

Using the K values determined, predictions of $pCOD_{\text{cellulose}}$ concentrations and $dCOD_{\text{glucose}}$ concentrations were made.

B.3 Modeled $pCOD_{\text{cellulose}}$ and $dCOD_{\text{glucose}}$ Values

Using the Cellulose Removal equation, Equation 3.16 was rearranged to determine effluent $pCOD_{\text{cellulose}}$ concentrations. Actual influent $pCOD_{\text{cellulose}}$ concentrations were input into Cell 1, and the effluent $pCOD_{\text{cellulose}}$ concentration was used as influent to Cell 2. This method was followed for Cells 3 and 4 as well. The $pCOD_{\text{cellulose}}$ concentration results are shown in Table B.10 below.

Table B.10: Simulated pCOD_{cellulose} monthly concentrations in units of mg COD/L for Cells 1 through 4.

Date	Cell 1	Cell 2	Cell 3	Cell 4
Aug-12	185.7	141.4	86.0	57.7
Sep-12	223.7	163.2	117.8	62.8
Oct-12	171.0	182.8	125.2	113.2
Nov-12	228.8	241.6	153.1	132.8
Dec-12	259.9	268.3	171.1	141.6
Feb-13	269.2	412.5	180.7	155.0
Mar-13	232.3	246.3	197.0	164.7
Apr-13	218.3	314.1	268.5	332.9
May-13	223.7	250.1	257.6	289.5
Jun-13	226.9	193.7	145.8	237.9
Jul-13	292.3	261.5	300.6	330.1
Aug-13	138.6	2029	207.9	308.9
Sep-13	291.8	196.2	262.3	264.2
Oct-13	253.8	254.6	239.8	246.9
Nov-13	289.3	332.0	309.2	307.7
Dec-13	232.8	270.2	211.6	223.1
Jan-14	182.9	212.5	181.1	172.7
Feb-14	253.2	246.3	255.4	257.1
Mar-14	265.9	280.0	273.5	301.0
Apr-14	232.1	192.0	194.9	220.7
May-14	213.2	226.0	195.0	216.5
Jun-14	227.8	206.3	187.4	198.6
Jul-14	325.4	259.4	265.5	288.7

Once the pCOD_{cellulose} concentrations were modeled, those values were used in the rearranged Equation 3.15 to determine the dCOD_{glucose} effluent monthly concentrations. The simulated dCOD_{glucose} concentrations are shown below in Table B.11.

Table B.11: Simulated dCOD_{glucose} monthly concentrations in units of mg COD/L for Cells 1 through 4.

Date	Cell 1	Cell 2	Cell 3	Cell 4
Aug-12	160.4	160.9	156.6	156.1
Sep-12	158.3	135.9	137.2	137.4
Oct-12	196.9	188.7	156.6	149.2
Nov-12	183.2	134.9	165.2	151.5
Dec-12	177.1	144.3	153.0	115.2
Feb-13	235.9	131.1	261.0	238.0
Mar-13	191.9	174.0	189.3	185.9
Apr-13	185.3	120.4	136.3	102.1
May-13	172.6	124.6	123.1	99.2

Table B.11 Continued.

Jun-13	145.7	122.6	136.4	111.7
Jul-13	127.0	114.8	91.5	80.8
Aug-13	203.9	133.8	129.4	69.7
Sep-13	127.6	170.3	116.8	105.0
Oct-13	138.3	138.0	137.1	118.9
Nov-13	154.4	118.3	128.9	104.3
Dec-13	164.2	137.0	141.3	119.5
Jan-14	163.0	155.3	139.3	125.2
Feb-14	183.4	179.7	175.1	148.2
Mar-14	169.9	141.0	142.7	131.1
Apr-14	149.3	167.2	153.8	140.2
May-14	187.1	165.0	189.3	158.9
Jun-14	166.0	157.3	162.5	132.8
Jul-14	157.7	177.6	169.4	132.2